DEUTSCHES ELEKTRONEN-SYNCHROTRON DESY

DESY 77/52
August 1977

Recent Results on e^+e^--Annihilation at DORIS

by

Uwe Timm

NOTKESTRASSE 85 · 2 HAMBURG 52

To be sure that your preprints are promptly included in the
HIGH ENERGY PHYSICS INDEX ,
send them to the following address (if possible by air mail) :

DESY
Bibliothek
2 Hamburg 52
Notkestieg 1
Germany

RECENT RESULTS ON e^+e^- - ANNIHILATION AT DORIS

Invited talk at the EPS European Conference on Particle Physics, Budapest 1977

Uwe Timm
Deutsches Elektronen Synchrotron, DESY

Contents

I. Introduction

In this contribution recent results on e^+e^- annihilation are presented, which were obtained with detectors of very different but complementary designs at the storage ring DORIS.

The accelerator and storage ring complex DESY-DORIS is shown in fig.1. DORIS consists of two vertically separated rings which cross each other at two interaction points. The rings are filled in the following way: electrons are injected from the linear accelerator I into the synchrotron, accelerated to the desired energy and transferred to DORIS. Positrons are produced in the linear accelerator II by conversion of electrons striking a target; they are collected after the target and accelerated prior to injection into the synchrotron. Each ring can be filled with 480, 240, or 120 bunches, where the lower bunch numbers optimise the luminosity at higher energies. The double ring structure permits also to store particle combinations such as e^-e^- or e p, but in view of the exciting results from e^+e^- collisions those other combinations have not been used up to now. DORIS has been operated at total CMS energies between 3.0 and 5.2 GeV with a maximum luminosity of $2.10^{30} cm^{-2} sec^{-1}$ at mashine currents of about 200 mA.

The four detectors which have taken data at DORIS are described briefly in the following chapters. The majority of experimental results reported here comes, however, from data taken during the year 1976, where the detectors DASP and PLUTO occupied the two interaction regions and collected each a total integrated luminosity of about 6000 nb^{-1}.

The double arm spectrometer DASP(TH Aachen, DESY, Univ.Hamburg, MPI München, Univ.Tokyo) is a device which is partly magnetic, covering $0.072 \times 4\pi$ of solid angle, and which has a nonmagnetic inner part that subtends over $0.70 \times 4\pi$ sterrad. A top view of the detector is shown in fig.2. Each of the two identical spectrometer arms has three proportional wire chambers in front of the magnet and six spark chambers behind, which define the track of a charged particle. A particle further proceeds through a time of flight counter, a shower counter and a range counter with a scintillator array after 70 cm of iron absorber. Outstanding features are a high momentum resolution, $\Delta p/p = 0.007p$ (p in GeV/c) at 18 kGm, and an excellent particle separation, obtained by the TOF measurement, which separates pions from kaons up to 1.6 GeV/c, and kaons from protons up to 3.0 GeV/c. The energy resolution of the shower counters is $\Delta E/E = 0.30/\sqrt{E}$ (E in GeV). The inner detector is located in the field free region between the two magnets. A view

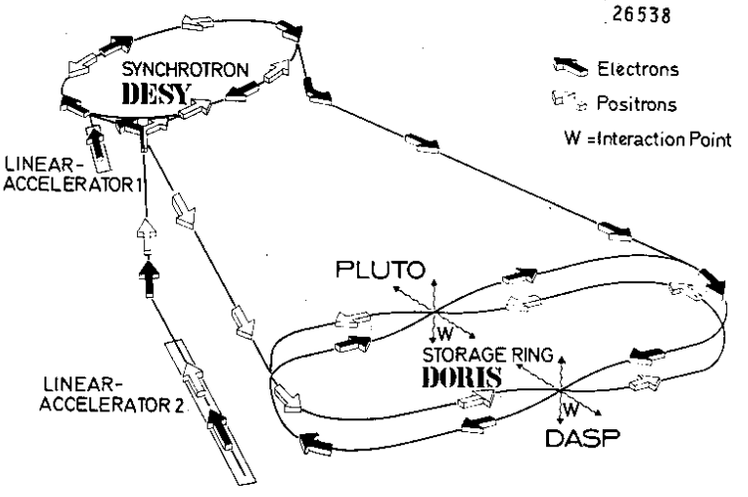

Fig.1 Schematic view of DORIS storage ring and injection system

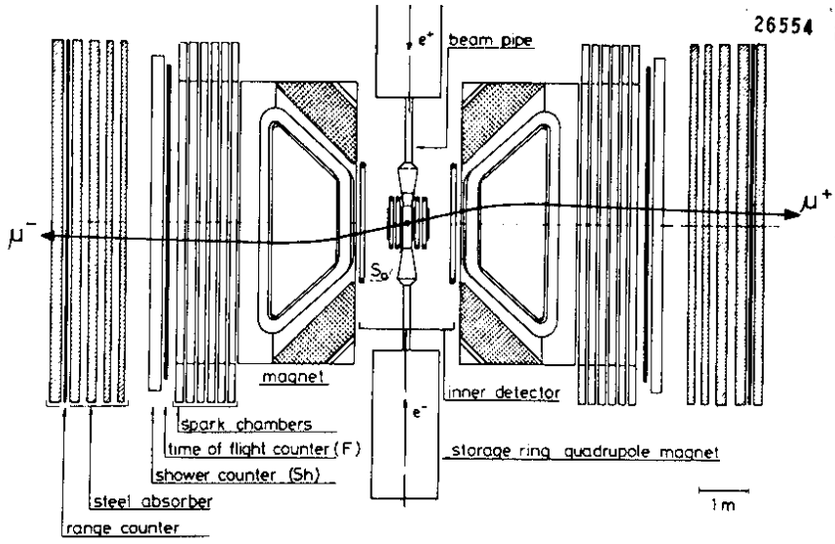

Fig.2 Top view of the double arm spectrometer DASP

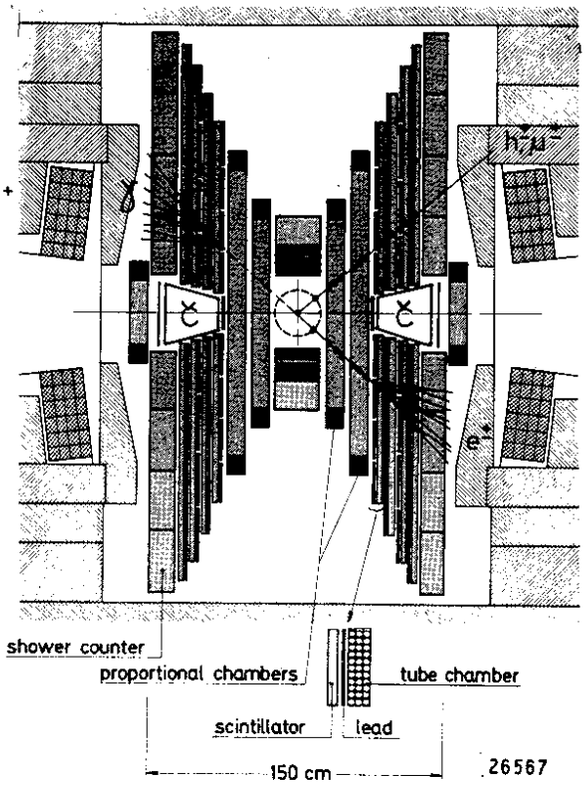

Fig.3 View of the inner detector of DASP

along the beam pipe is shown in fig.3. A particle from the origin penetrates four layers of sandwiches, consisting of scintillators, lead and proportional tubes, which measure the conversion points of photons, and a lead-scintillator shower counter. This detector determines the direction of charged particles and photons to within $\pm 2^\circ$ and gives an energy measurement for photons and electrons. Also shown are two Cerenkov counters which improve the electron separation in the outer arms considerably. The spectrometer is triggered on a single track, that penetrates to the shower counter. The inner detector can be triggered either on the number of tracks or photons seen, or on the amount of energy deposited. DASP provides a precise momentum determination and a good particle separation in a limited solid angle and measures the directions of charged particles and photons in a large part of 4π.

A completely magnetic device with 'full' solid angle coverage is the solenoid PLUTO (DESY, Univ. Hamburg, Univ.Siegen, Univ.Wuppertal), as shown in fig.4. It has a superconductive coil with a usable volume of 1.4 m diameter and 1.05 m length. The maximum magnetic field is 20 kG. The inner region is filled with 14 cylindrical proportional chambers. Two lead converters are inserted at radii of 37.5 cm and 59.4 cm which have a thickness of 0.44 and 1.72 radiation length respectively.

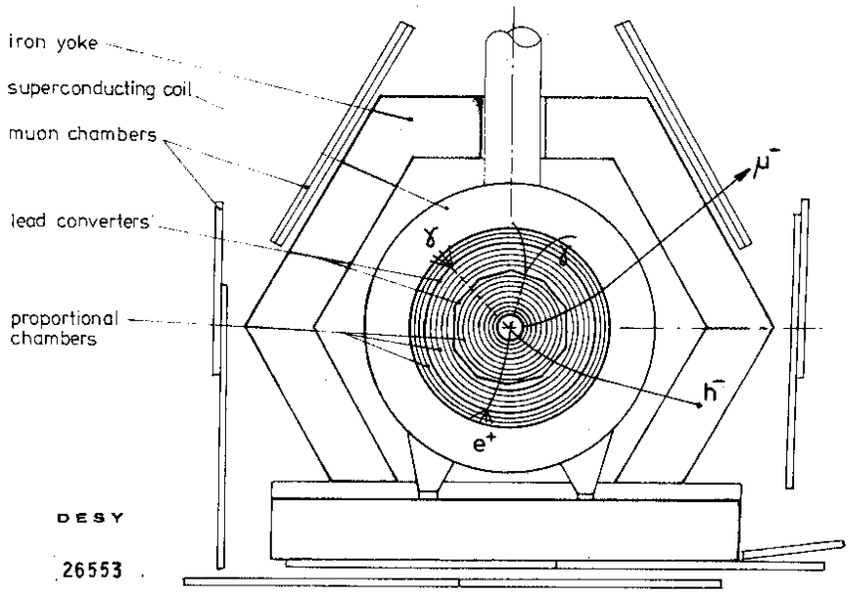

Fig.4 View of the solenoid detector PLUTO

They allow the detection of photons by pair- or shower production, and also the separation of electrons from hadrons. The momentum resolution $\Delta p/p = \pm 0.06$ at 1.5 GeV/c is still dominated by multiple scattering in the chamber walls and lead converters. Muons are identified in proportional tube chambers on the yoke surface, where the iron acts as filter against the hadrons. The detector is triggered by a wire logic on two or more tracks in $0.86 \times 4\pi$ solid angle. The solid angles covered for the detection of charged tracks, electrons or photons, and muons are 0.94, 0.56 and $0.50 \times 4\pi$ respectively. The

outstanding feature of PLUTO is the clean identification of muons. The momenta of charged particles are measured with moderate accuracy in a large solid angle. Electrons and photons are separated.

A nonmagnetic detector, DESY-HD (DESY, Univ.Heidelberg), is shown in fig.5. The beam pipe is surrounded by cylindrical drift chambers, followed by NaJ- and lead glass counters, cosmic ray counters, and an iron shield which is covered by a layer of muon chambers. A cylinder filled with mercury of two radiation lengths thickness in front of the last drift chambers, which can be filled or emptied between runs, acts as photon converter. Solid angles covered for detection of muons, electrons or photons, and charged particles are 0.32, 0.45, and $0.95 \times 4\pi$ respectively. Energy resolutions are $\Delta E/E = 0.11$ at 1 GeV (FWHM) for NaJ and $\Delta E/E = 0.30$ at 1 GeV (FWHM) for lead glass. The event trigger can be varied according to the desired number of visible charged tracks, and the amount of energy deposited in the counters. The detector measures directions of charged particles and photons, and distinguishes leptons and photons from hadrons. Events with up to four tracks or showers can be reconstructed kinematically from the particle directions.

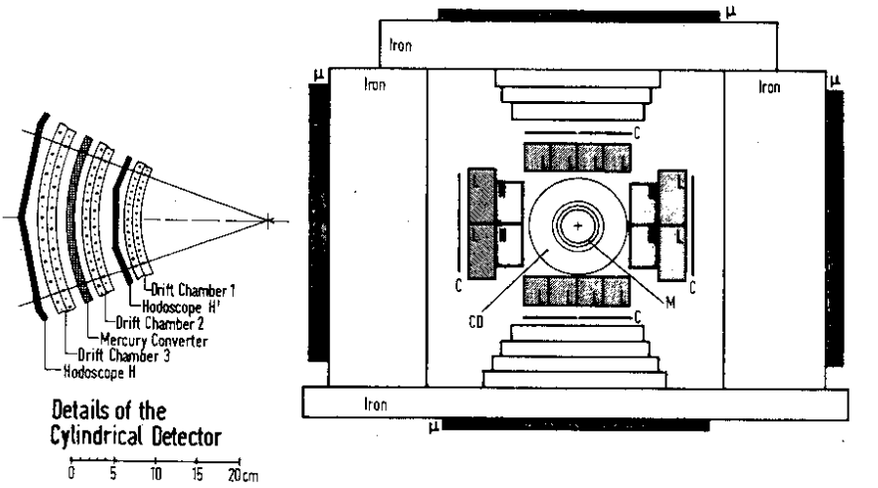

Fig.5 Neutral detector DESY-HD, N = NaJ, L = leadglass, C = cosmic c.

The other non magnetic detector at DORIS is specialised in the detection of neutrons and antineutrons: BONANZA (Univ.Bonn, Univ.Mainz). It is shown in fig.6 in a view perpendicular to the beams. Four cylindrical proportional chambers allow the tracking of charged particles.They are surrounded by veto counters, by a square shaped ring of neutron counters and by another ring of veto counters. Also the endfaces are covered by veto counters as indicated. The fig.7 shows the star from an antineutron obtained in a run taken early this year at DORIS. The event is traced by a precise measurement of energy deposit and time of passage, $\sigma_{\Delta t} = 0.4$ nsec, through the various counters. $\beta = 0.81 \pm 0.6$ for the $\bar{n}$ is derived from a beam crossing signal.

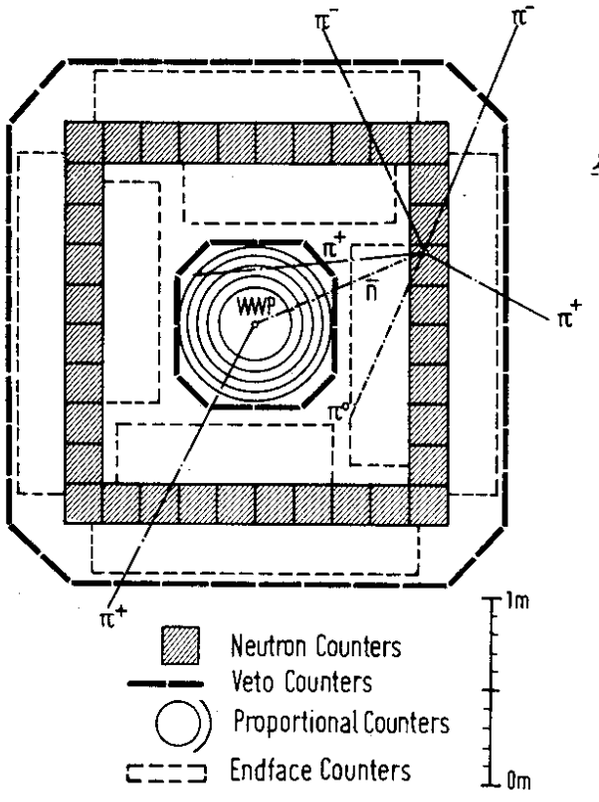

Fig.6 The neutral detector BONANZA, designed for detection of neutrons and antineutrons

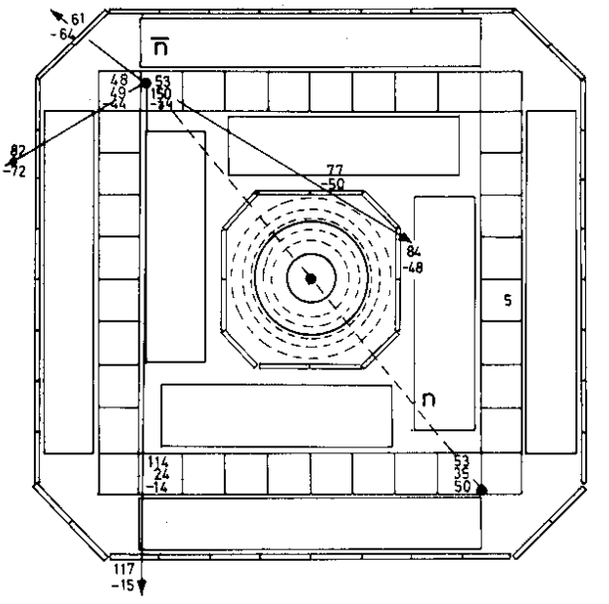

Fig.7 Computer output of a $\bar{n}n$- event in the detector BONANZA. The small numbers indicate z-coordinate, energy deposit, and relative time of passage in the neutron counters, for the veto counters the energy deposit is not measured.

II. Spectroscopy of the resonances $J/\psi(3.1)$ and $\psi'(3.7)$

Decays of the resonancea have been observed in different modes. With the DASP detector the three photon final state has been analysed, using events from the inner detector. The detector DESY-HD investigated the $\gamma\gamma\pi^+\pi^-$ channel, and results from PLUTO concern the decays $J/\psi \to \pi^+\pi^-\pi^+\pi^-\pi^0$ and $\psi' \to \gamma\gamma J/\psi$. The branching ratios and decay widths measured are collected in table 1 and table 2. The data in the tables are selected according to the aim of this talk, which presents the more recent results from DORIS experiments. In the following only some important decays of the list will be discussed here.

The analysis of the three photon final state requires the three showers to lie in a plane with the interaction point. Compared to earlier results [1] the data reported here are based on more statistics and a new study of the QED background. There are two kinematic solutions for the invariant two photon mass. The low mass solution is shown in fig.8. The solid line is a fit to the data with η and η', which includes the background as indicated. The resulting branching ratios $J/\psi \to \gamma\eta$, and $J/\psi \to \gamma\eta'$ are listed in table 1. The rather large error in the latter decay results from the low fraction of the decay $\eta' \to \gamma\gamma$ of 2%. The DESY-Heidelberg group [2] observed the η' also in the decay mode $\gamma\varrho^0$ with 30% fractional decay. The invariant mass distribution, $M(\gamma\pi^+\pi^-)$ is shown in fig.9. The shaded area is a result of cuts which reduce the background below the η' signal by excluding the π^0 mass and restricting the $\pi\pi$ mass to the ϱ^0 region.

There is improved evidence [1] for the exsistance of the state X(2.8) in the decay $J/\psi \to \gamma X \to \gamma\gamma\gamma$. Fig.10 shows the high mass solution of the three photon mode, where the solid line is the result of a fit which includes the background as indicated. It yields a mass $M_X = 3.83 \pm 0.03$ GeV. The evidence for this state, supposed to be the expected speudoscaler η_c', is now a 5 standard deviation effect.

Most of the decay widths listed in table 1 lie between 50 and 500 eV. Small widths are in fact expected on the basis of the OZI rule [3]. There have been attempts [4] to arrive at more quantitative predictions by assuming SU(4) breaking which, with a 10^{-4} admixture of $c\bar{c}$ to the final state particles is partly successful to predict the decay $\varrho\pi$ with $\Gamma_{\varrho\pi} = 600$ eV, whereas the radiative decays come out much too high : $\Gamma_{\gamma\eta} = 670$ eV, $\Gamma_{\gamma\eta'} = 3600$ eV (see list). Note that three decays of table 1 have much smaller widths than the rest. In the $c\bar{c}$ - mixing model, the small width of the channel $\gamma\pi^0$ is understandable since such a component in the π^0 is forbidden by isospin. The measured rate also agrees roughly with a value predicted from the vector dominance model [5]. For the direct decay $J/\psi \to \gamma\gamma\gamma$ only 5 events were found, yielding the upper limit of $\Gamma_{\gamma\gamma\gamma} < 5.1$ eV quoted. This low

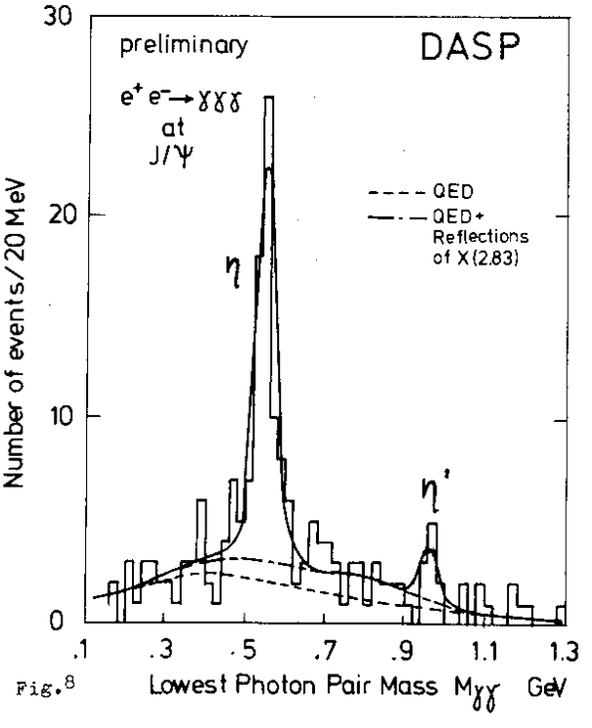

Fig.8

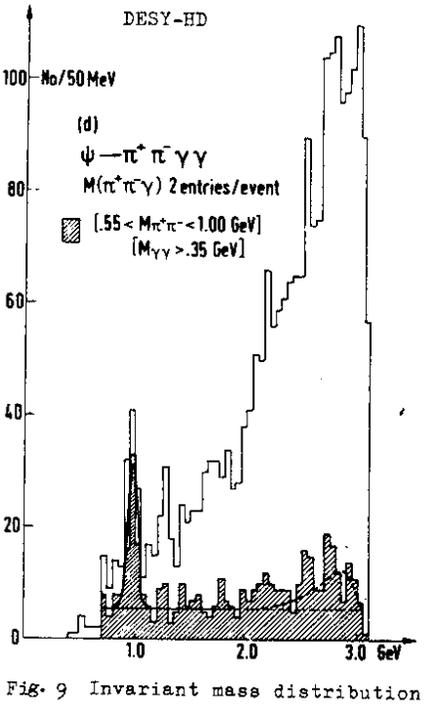

Fig. 9 Invariant mass distribution $\pi^+\pi^-\gamma$

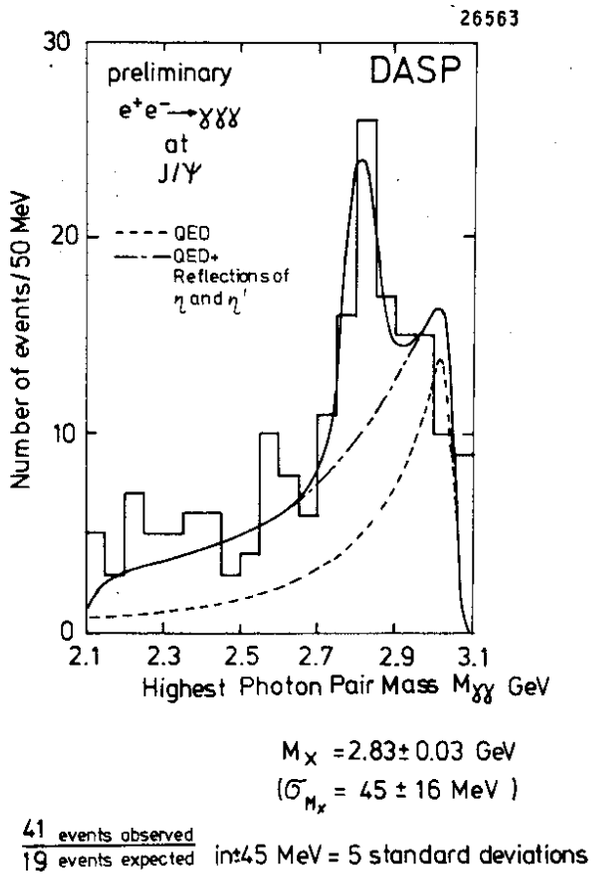

Fig.10 Distribution of the high $\gamma\gamma$ mass

Table 1

List of branching ratios $J/\psi \to f$

channel f	BR x 10^3	Γ (eV)	detector
$\gamma\pi^0$	0.073 ± 0.047	5.0 ± 3.2	DASP
$\gamma\eta$	0.80 ± 0.18	55 ± 12	DASP
	1.3 ± 0.4	91 ± 28	DESY-HD
$\gamma\eta'$	2.2 ± 1.7	152 ± 117	DASP
	2.4 ± 0.7	165 ± 48	DESY-HD
γX	0.12 ± 0.05	8.3 ± 3.5	DASP
$\gamma\gamma\gamma$	< 0.078	< 5.1	DASP
3π	10.0 ± 2.0	690 ± 138	DESY-HD
$\omega\pi^+\pi^-$	7.8 ± 1.6	543 ± 100	PLUTO
ωf	4.0 ± 1.4	276 ± 96	PLUTO
$B^\pm\pi^\mp$	2.8 ± 0.7	193 ± 47	PLUTO

width is in good agreement with a prediction[6] where the decay rate should be proportional to the sixth power of the quark charges. For unit charges the prediction is $\Gamma_{\gamma\gamma\gamma}$ = 30 eV, much above the experimental value. For a charge 2/3 however, one expects 2.6 eV. There is no explanation up to now for the small decay width $\Gamma_{\gamma X}$. Moreover, no other decay channels of the X(2.8) have been observed besides the two photon transition. The only conclusion as to the nature of this state is that its spin is $J \neq 1$, and its G-parity is positive. The assignment as $\eta_c' = {}^1S_0$ causes difficulties because of its small coupling to the J/ψ.

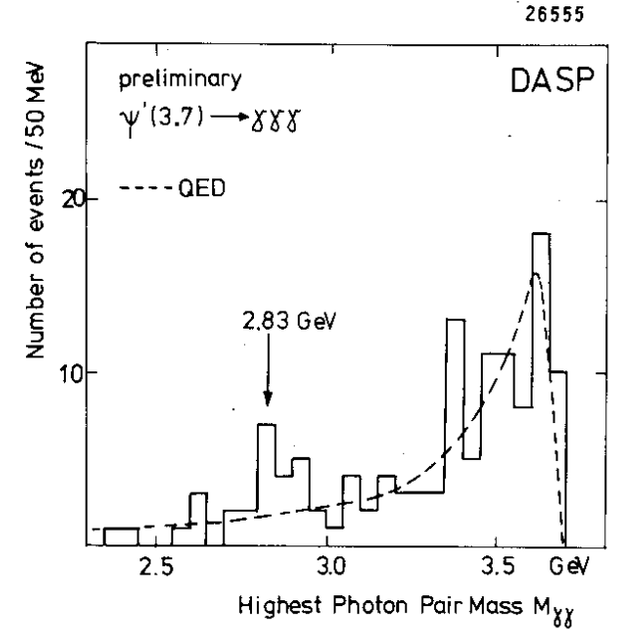

Fig.11 Distribution of the high $\gamma\gamma$ mass

The three photon final state has also been investigated at the ψ' with the neutral detector DESY-HD [2] and the DASP inner detector [7]. Table 2 shows that none of the decay channels listed have been observed. The upper limits of the product of branching ratios have 90% confidence. The decay $\psi' \to \gamma X(2.8)$ would appear as a peak in the high mass spectrum, centered around $M_{\gamma\gamma}$ = 2.83 GeV. The present experimental evidence is shown in fig.11 It suggests,

Table 2

List of upper limits $\psi' \to f$

channel f	BR($\psi' \to \gamma h$) x BR($h \to f$)	detector
$\gamma\eta \to \gamma\gamma\gamma$	$< 1.6 \times 10^{-4}$	DASP
$\gamma\eta' \to \gamma\gamma\gamma$	$< 1.2 \times 10^{-4}$	DASP
$\gamma X(2.8) \to \gamma\gamma\gamma$	$< 3.4 \times 10^{-4}$	DASP
$3\pi \to \gamma\gamma\pi\pi$	< 10	DESY-HD
$\gamma\chi(3.41) \to \gamma\gamma\gamma$	$< 4.0 \times 10^{-4}$	DASP
$\gamma\chi(3.45) \to \gamma\gamma\gamma$	$< 3.1 \times 10^{-4}$	DASP
$\gamma P_c(3.51) \to \gamma\gamma\gamma$	$< 2.6 \times 10^{-4}$	DASP
$\gamma\chi(3.55) \to \gamma\gamma\gamma$	$< 2.0 \times 10^{-4}$	DASP

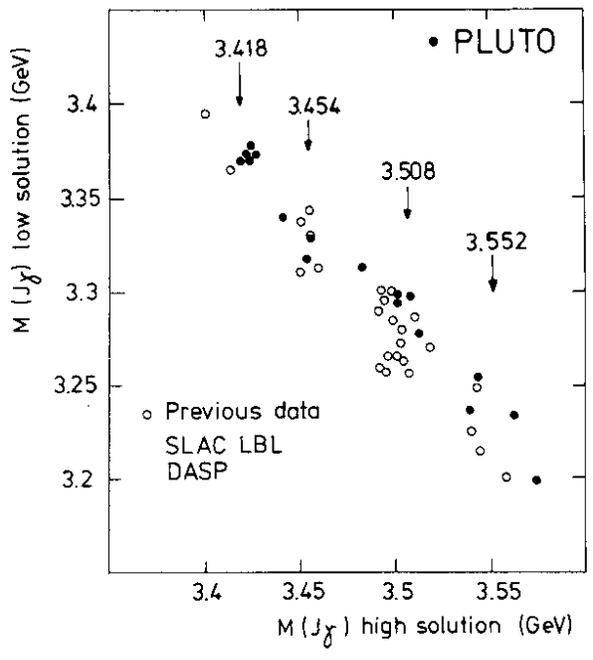

Fig.12 High mass($\gamma J/\psi$) vs. low mass, from the reaction $e^+e^- \to \mu^+\mu^-\gamma\gamma$ at $\psi'(3.684)$, $M(\mu^+\mu^-)$ constrained to J/ψ, $M(\gamma\gamma)=\eta$ excluded.

that with more statistics the upper limit given in table 2 for this decay might turn into an observed branching ratio.

Two photon decays have not been observed for any of the states with even charge conjugation below the ψ', but all are seen as radiative cascade decays $\psi' \to \gamma\chi \to \gamma\gamma J/\psi$ at DORIS in the DASP detector [8], at SPEAR by the SLAC-LBL group [9], and by the MP^2S^2 group [10] with the exception of the $\chi(3.45)$. Fig.12 shows the result of a new experiment in the superconductive solenoid PLUTO [11], where one or two photons have been observed accompanied by two muons from the decay $J/\psi \to \mu^+\mu^-$. All four states show up in the high $(J/\psi,\gamma)$ mass; in particular the evidence for the decay $\chi(3.45) \to \gamma J/\psi$ is improved by three more data points. The branching ratio for this decay, however, is still unknown.

Another experimental result from PLUTO concerns the inclusive production of J/ψ-mesons in the energy region $4.0 < \sqrt{s} < 5.0$ GeV [12]. There have been speculations that 'charm-molecules' i.e. bound states of four quarks $(q\bar{q}c\bar{c})$ may exist [13]. In particular the $c\bar{c}$ - contributions of the enhencements in the total cross section for e^+e^- annihilation at $\sqrt{s} = 4.03$ and 4.4 GeV are attributed to the formation of such states [14]. Most of the models predict branching ratios of the order 10^{-1} for the decay into J/ψ and hadrons. Fig.13 shows (right diagram) that the cross section observed for the production of inclusive J/ψ mesons is 10^{-3} below the total cross section. Only four events are seen, but none at the resonances 4.03 or 4.4 GeV. The left part of the diagram shows the expected (solid line) and measured cross section for J/ψ production from the radiative tail of the ψ'. These events can be clearly identified by kinematic fits (12 events). The level of inclusive J/ψ production is thus compatible with the expected violation of the OZI rule [3].

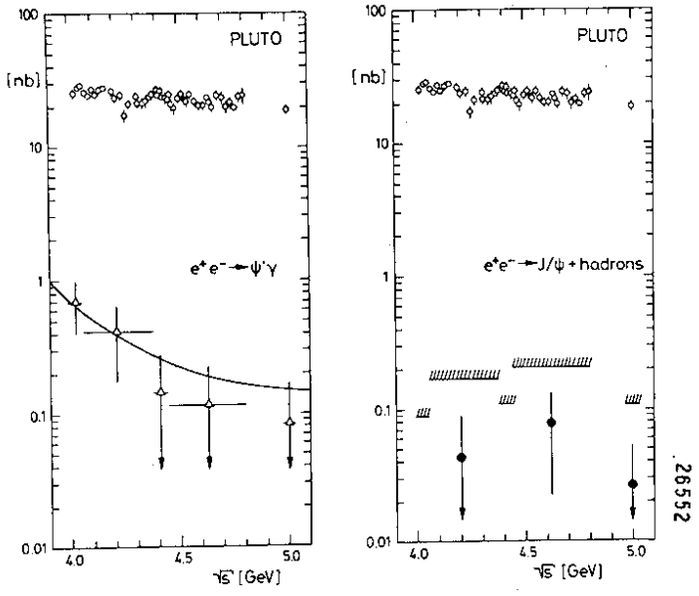

Fig.13 Inclusive J/ψ-production between 4.0 and 5.0 GeV. Left: background from radiative tail of ψ', calculated and measured, Right: inclusive events (four) and upper limits (hatched bars).

III. The total hadronic cross section and hadronic spectra

The large solid angle for the detection of charged tracks makes the superconductive solenoid PLUTO an ideal instrument to measure the total e^+e^- annihilation cross section. The published data [14] have been reanalysed and more data were taken up to 5.0 GeV. The present result is presented in fig.14. Radiative corrections are applied. The error bars are not purely statistical but include the error due to the unfolding procedure of the prong classes. The systematic error quoted by the authors is 11%, including the error for the Monte Carlo simulation ($\approx$10%), and for the small angle Bhabha scattering monitor (5%). The efficiency to detect multiprong events in the detector is 90%, for twoprongs it is 40%. The figure is lower because of the cuts necessary to remove the large QED - background, which dominates in the twoprong class. The Monte Carlo simulation uses the jet model with an angular distribution of the jet axis $\sim 1 + \cos^2\Theta$, and an average transverse momentum of $\langle p_T \rangle$ = 350 MeV/c. It requires in its present form as an all pion model a 1 : 1 ratio for charged to neutral pions, and uses a 15% contribution of kaons. The jet model is clearly favoured over the isotropic phase space distribution, as seen by comparing the angular distribution of hadronic tracks. This is shown in fig.15, where the number of tracks observed divided by the number of tracks simulated is plotted per bin in cos Θ for $\sqrt{s}$ = 5 GeV. The ratio must be 1 for a successful simulation, case B. Studies of the sphericity, the asphericity, and the prolaticity [15] of the PLUTO events show that the angular distribution is the most sensitive test at 5 GeV for the jet model, because effects of the limited transverse momenta are not much pronounced in the energy range of these data between $\sqrt{s}$ = 3.6 and 5.0 GeV. Fig. 16 shows the fraction $\mathcal{E}$ of the total energy observed, assuming the particles are pions, compared to the assumptions of the Monte Carlo simulation, which are in good agreement. No data were taken between $\sqrt{s}$ = 3.7 and 4.0 GeV. As fig.14 shows, there is a large step from R$\approx$2 near 3.6 GeV up to R$\approx$5 at the first resonance at 4.03 GeV, which is attributed to the production of charmed D mesons [16] above the charm threshold. The normalised cross section then stays at the higher level around R$\approx$4.5 with resonances at 4.15 and 4.4 GeV, there may be other unresolved resonances. The shaded areas in fig.14 are intented to indicate that the data are in general agreement with the expectation of the triplet quark sum rule, if the new heavy lepton is taken into account. For the area marked as R^{old}, the sum rule yields $R^{old} = 3\cdot\sum q_i^2 = 2$ (q_i = quark-charges, i = u,d,s). The cross section of the heavy lepton, R_τ, follows the threshold behaviour of a pointlike fermion above 3.8 GeV (see section V) and approaches one unit in R at high energies. For the production of charmed mesons above 3.73 GeV the sum rule predicts an increase $R^{new} = 3q_c^2 = 1.33$ where the threshould behaviour is not quite clear. The excess of the experimental cross section of R$\approx$0.5 above the predicted level beyond $\sqrt{s}$ = 4.5 GeV may be due to resonant behaviour or simply a systematic effect in the data. Note that the data around 3.6 GeV have also an excess of $\approx$10% above the predicted $R^{old} = 2$. In the presence of the heavy lepton the cross section plotted is no more purely hadronic, but contains a leptonic contribution.

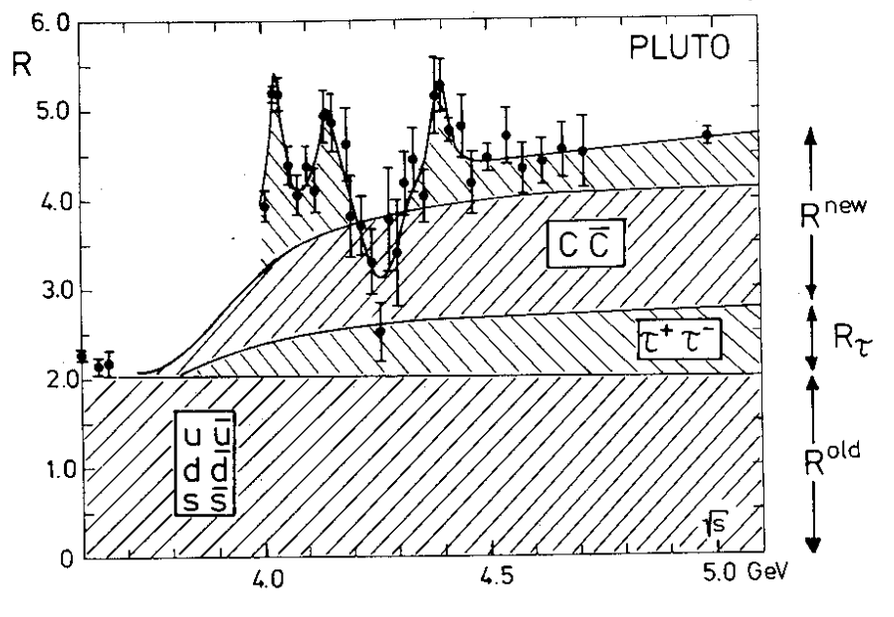

Fig.14
The total cross section for e^+e^- annihilation in units of $R = \sigma_{tot}/\sigma_{\mu\mu}$
$\sigma_{\mu\mu} = 4\pi\alpha^2/3s = 86.84/s$ nb.

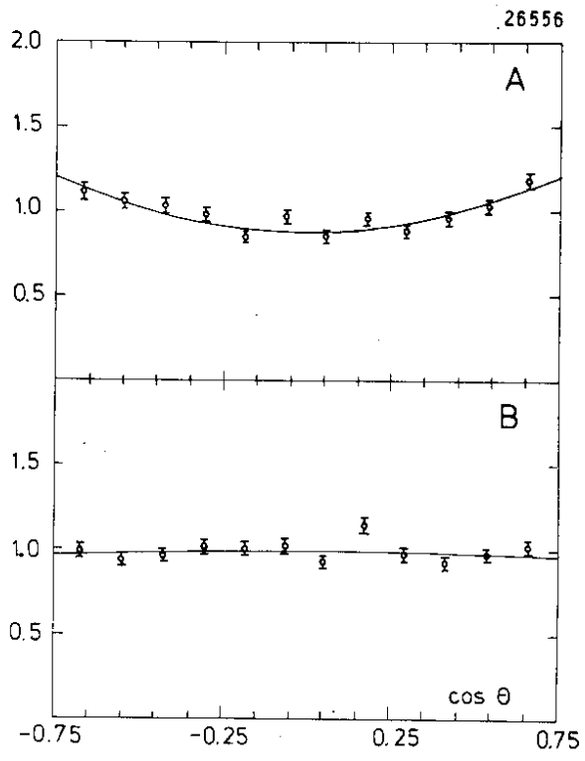

Fig.15 Angular distribution of hadron tracks
A. Normalized to phase space distribution
B. Normalized to Jet Model (α_{mod}=1) Plot(76)
$\sqrt{s}$ = 5 GeV

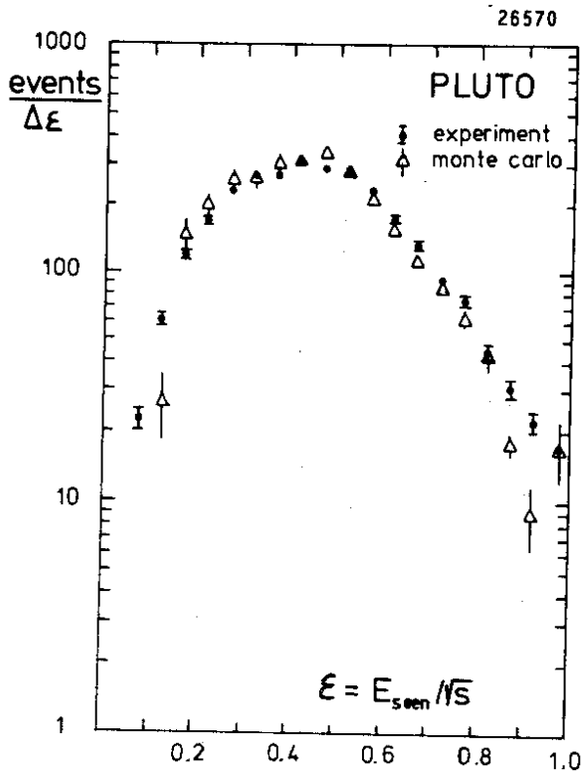

Fig.16 Fraction ε of total energy seen at $\sqrt{s'}$ = 4.5 GeV, compared to the Monte Carlo expectation.

As to the resonant structure, the PLUTO data are in good agreement with the total cross section measured by the SLAC-LBL group [17], these data are, however, higher by 10 - 15% in the lower energy region up to 4.5 GeV. Fig.17 shows the measured two prong cross section, in units of R. It reproduces the structure of the total cross section, and thus constitutes a roughly constant, ~30%, and large fraction of the total cross section. If the contribution of the heavy lepton τ, which has a large two prong fraction of decays, is subtracted, there remains still an appreciable amount of two prong events in the charm region, also at the resonances. The average multiplicity of charged prongs as function of s has a smooth logarithmic dependence with $\langle n_{ch} \rangle \approx 4$ in the rgion $\sqrt{s'}$ = 3.6 to 5.0.

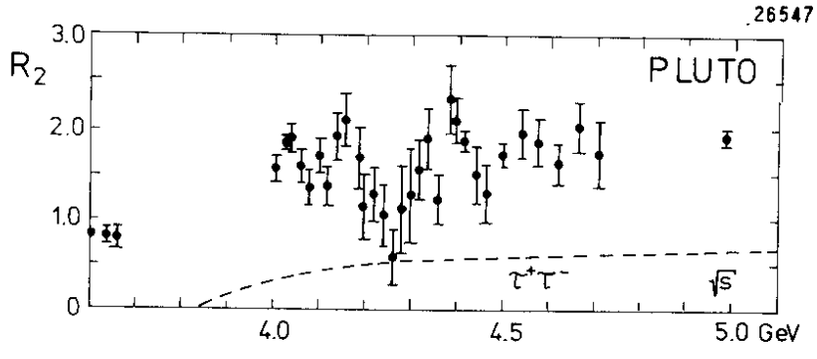

Fig.17 Two prong cross section $R_2 = \sigma_2/\sigma_{\mu\mu}$. The dashed line is the contribution of the heavy lepton τ.

The data taken in the energy region $\sqrt{s'}$ = 3.6 to 5.0 GeV have been analysed for the distribution of momenta of the final state particles. If scaling holds, one expects [18] a dependence $s^{\beta} \cdot d\sigma/dx_E \sim x_E \overline{W}_1(x_E)$, where $x_E = 2E_h/\sqrt{s'}$ (h = hadron), independent of s. If only the momenta of the hadrons are measured, instead of x_E the variable $x_p = 2p_h/\sqrt{s'}$ is used. They disagree only at the low momenta. Fig.18 shows the hadronic spectra for energies $\sqrt{s'}$ = 3.6, 4.03, 4.5, and 5.0 GeV as function of x_p.

Data points below $x_p = 0.15$ have been omitted because they do not match with the Monte Carlo simulation. The simulation fits the data perfectly except for the region near the lowest momenta triggered, that is 0.24 GeV/c. There is a large increase of the differential cross section between $\sqrt{s} = 3.6$ and 4.03 GeV for the lower momenta, $x_p < 0.5$. This indicates, that the step in the total cross section at the same energy is due mainly to low momenta particles. Above $\sqrt{s} = 4.03$ the data have a common exponential decrease, $\exp(-b \cdot x_p)$, independent of s, beyond $x_p > 0.2$, which is the expected feature of scaling. The line in fig.18 is handdrawn and represents a slope $b = 7.56$. The data agree well with hadron spectra measured in the DASP detector [18]. This is shown in fig.19, where the line is repeated for comparison. There is a discrepency with the same spectra measured by the SLAC-LBL group [19] for $x_p > 0.5$. Fig.20 shows the spectrum of charged pions measured in the DASP detector [18] as function of the true scaling variable x_E, which again confirms scaling. The slope of the line is $b = 8.80$.

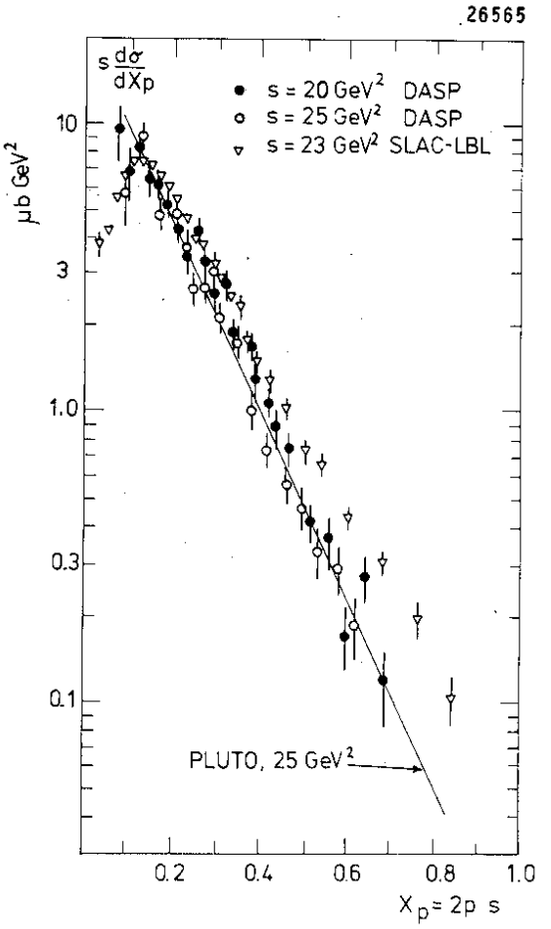

Fig.18 Momentum spectra of hadrons, PLUTO

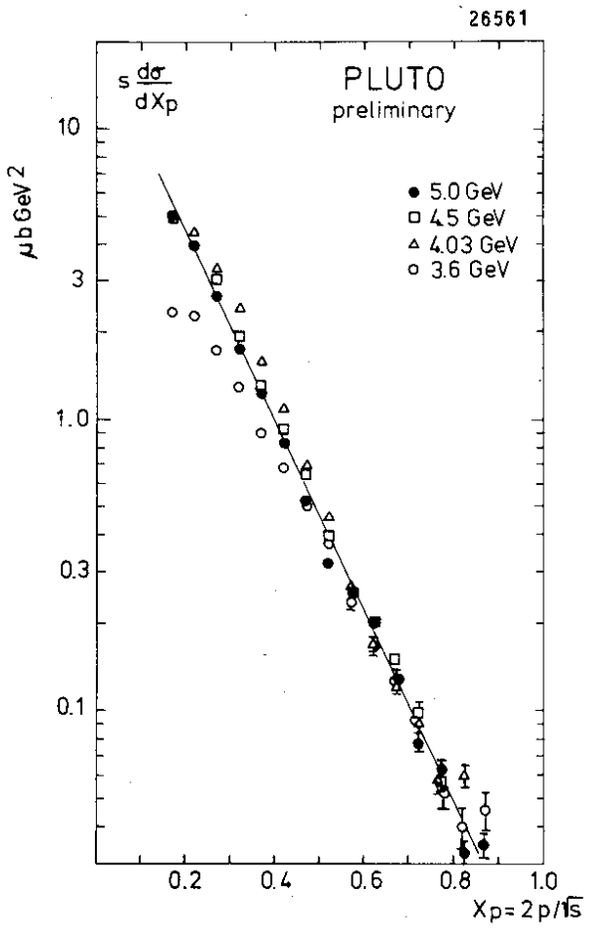

Fig.19 Momentum spectra of hadrons, DASP, SLAC

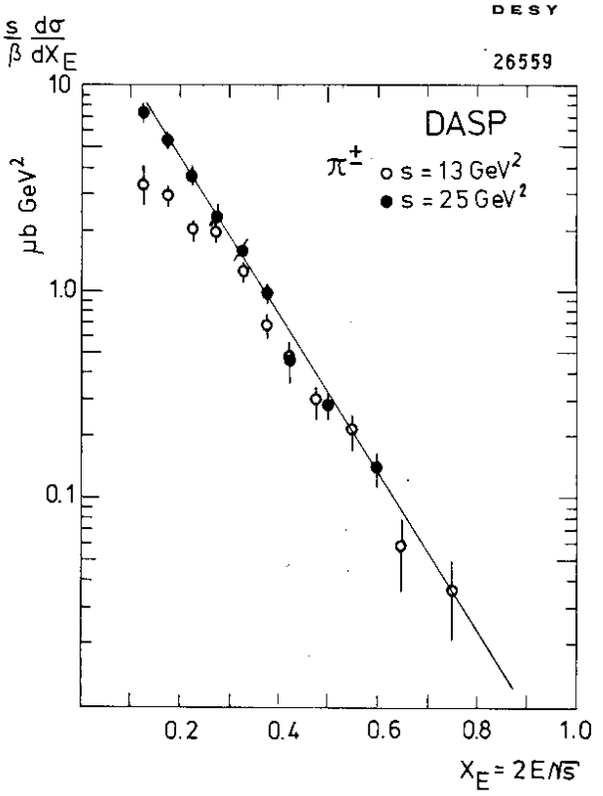

Fig.20 Energy spectra of charged pions, DASP

The data from the PLUTO detector have been investigated further by analysing the invariant mass of two hadrons, considered as pions. The mass spectrum obtained is shown in fig.21a, where the lower histogram represents the uncorrelated background from the combination of pions of two different events. In fig.21b the uncorrelated background is subtracted. A clear signal at the energy of the rho mass is visible. The peak near 0.5 GeV is from K^0_s-production and a reflection of the ω-meson, the large enhencement at 0.28 GeV is due to misinterpreted electrons from photon conversion in the beam pipe. The lefthand shoulder of the rho peak is lifted by a broad underlying signal of the K* reflection. The spectrum is very similar to the $\pi\pi$mass-distribution obtained from the SFM detector at the CERN ISR in inelastic pp-collisions [21], taken at $\sqrt{s}$ = 53 GeV. An analysis of this spectrum yielded dominant production of vector mesons, which accounts for more that 60% of all pions produced. The solid and dashed lins in fig.21b are the result of a fit with the known shape of the rho resonance to the data. The figs.21 contain all energies between 3.6 and 5.0 GeV. In fig.22 the preliminary cross section for inclusive ϱ^0- production is plotted versus $\sqrt{s}$, in units of R. It increases from R≈0.8 at 3.6 GeV to R≈1.3 above the charm threshold. Adding the inclusive cross sections for ϱ^+ and ϱ^- one arrives at R≈3.9, which suggests that a large fraction of rho mesons are produced primarily, whose decay pions feed the hadronic spectrum, fig.20, at lower energies. Fig.23 shows the preliminary energy spectrum of inclusive ϱ^0- production. Note that the data point at x_E = 0.93 has an additional large systematic error (dashed).

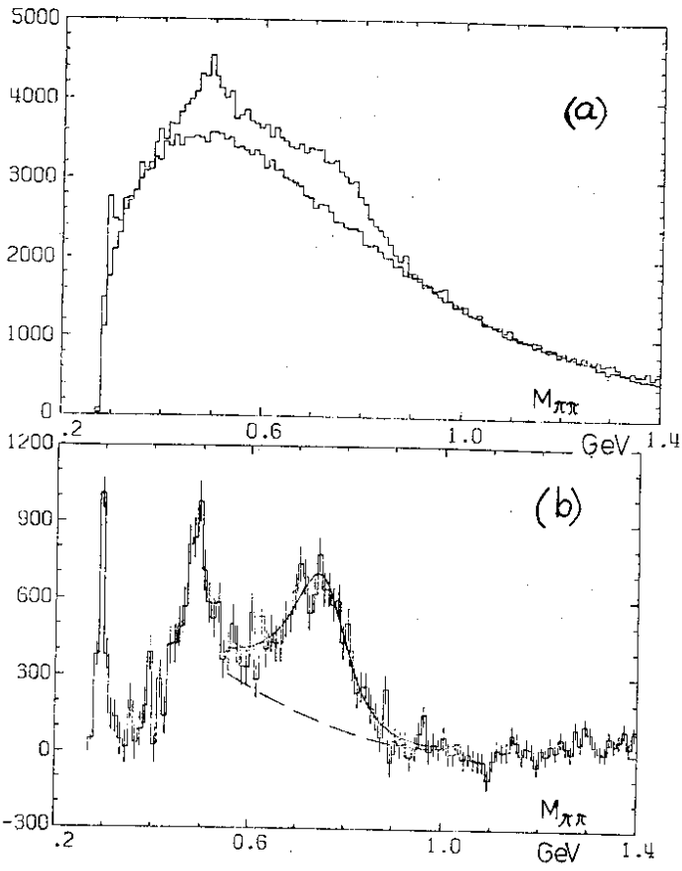

Fig.21 (a) Invariant mass spectrum $\pi^+\pi^-$
(b) Background subtracted.

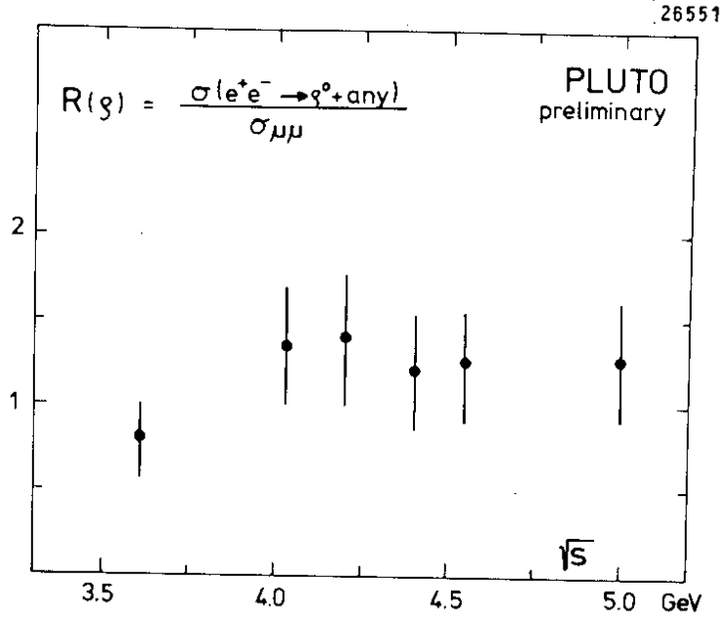

Fig.22 Inclusive cross section for ϱ^0 production, units R.

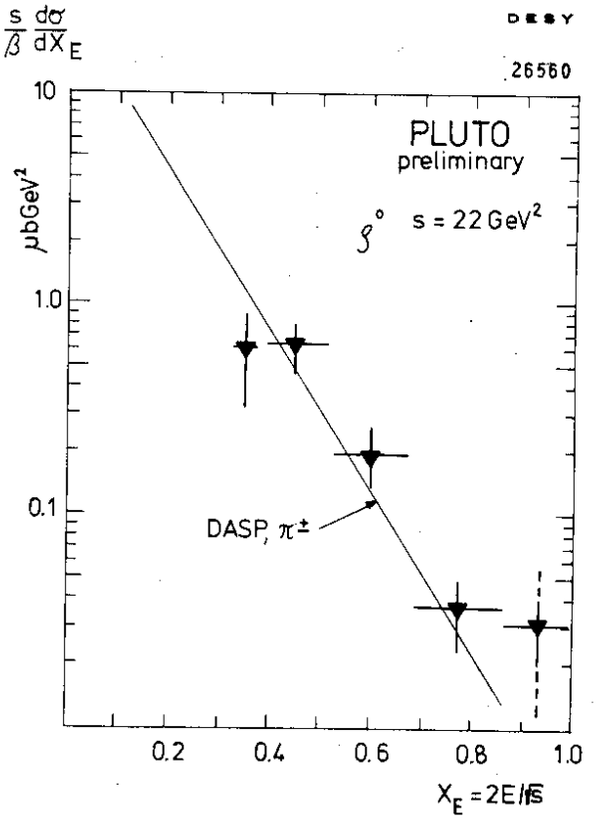

Fig.23 Energy spectrum for inclusive ϱ^0.

The data lie within errors on the slope of the charged pion spectrum shown in fig.20 (full line), the expected inclusive $\varrho^{\pm}$ - spectrum is therefore a factor of two higher. The dominant production of vector mesons at high x_E , now observed also in e^+e^- collisions, has a simple interpretation in the conventional quark model [22] which, based on spin and statistical arguments, predicts that the majority of all observed particles be decay products of vector meson resonances, having spin and parity $J^P = 1^-$.

IV. Experimental Evidence for Charm

Before discovery of the J/ψ all hadrons could be built from three quarks, s,u,d, a status which we have described as "old physics" in chapter III. The concept of a fourth quark with quantum number $c = \pm 1$ (charm) was introduced much before the discovery of the new particles in an attempt to achieve symmetry between leptons and quarks [23] , and later in order to explain the absence of neutral strangeness changing currents [24] by inventing the GIM mechanism, named after the initials of the three authors. While the decays of J/ψ and ψ' reported in chapter II deal with $c\bar{c}$ - states, which have charm quantum number zero (hidden charm), this chapter covers the evidence found in DORIS experiments for the existance of states with non vanishing charm quantum number. By introducing a new quark the scheme of hadrons is generalised from SU(3) to SU(4), which is illustrated in fig.24 for the case of pseudoscalar mesons. We find the "old" pseudoscalar mesons π^-, K^0, K^+,π^+, $\bar{K}^0$, K^-,(π^0,η,η') in the middle plane, $c = 0$, and the"new mesons" D^+, D^0, F^+ with $c = +1$ above, D^-, $\bar{D}^0$, F^- with $c = -1$ below this plane. The F^-- meson carries in addition to charm also strangeness $s \neq 0$. To prove the existance of charmed particles one has to find their characteristic weak decays. As a consequence of the GIM mechanism mentioned above the relative rate of decays of the charm quark into strange and non stange particles is given by the ratio $\cos^2\theta_c/\sin^2\theta_c = 1 : 0.05$, where θ_c is the Cabbibo angle.

Table 3. Decays and relative decay rates of D^0- mesons

$\cos^2\theta_c$ 1	$\cos^2\theta_c$ 1/20	
$D^0 = c\bar{u} \to K^- + \pi^+$	$D^0 = c\bar{u} \to \pi^- + \pi^+$	hadronic decays
$D^0 = c\bar{u} \to K^- + e^+ + \bar{\nu}_e$	$D^0 = c\bar{u} \to \pi^- + e^+ + \bar{\nu}_e$	semi leptonic decays

There are hadronic and semi leptonic decays. Table 3 illustrates the situation for the example of a decaying D^0- meson, from which we draw the following general conclusions, keeping in mind that the mesons are produced in pairs with e^+e^- collisions and that many more channels are open than shown in the table by picking up $q\bar{q}$ states from the vacuum.

(1) Neglecting the 5% non strange contribution, we expect two kaons per charm event,

(2) We expect the kaons correlated with electrons (muons) from the semi leptonic decays,

(3) At least in comparison with the heavy lepton (chapter V), one expects a high multiplicity of charged prongs,

(4) as a consequence of (3) the spectrum of electrons (muons) should be soft.

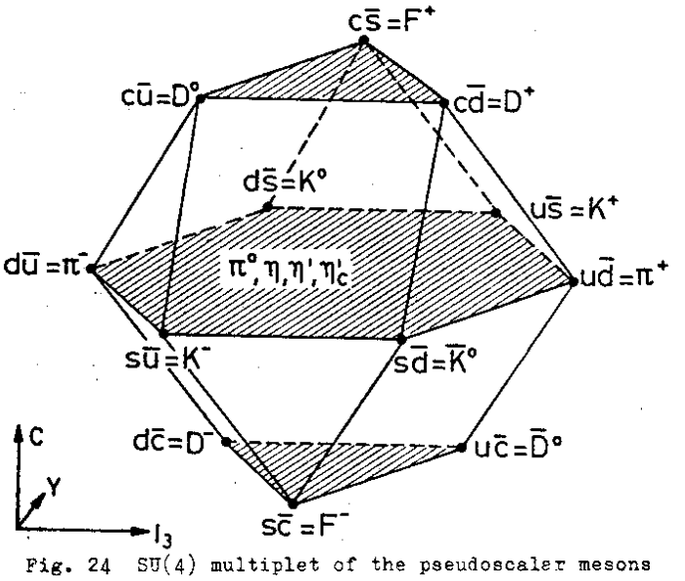

Fig. 24 SU(4) multiplet of the pseudoscaler mesons

The association of electron and strange particle , which is a characteristic signum for charm, was first shown by an experiment in PLUTO where the K^0_s mass was reconstructed from the invariant two pion mass of opposite charge, as shown in fig.25.

The events found in the K^0_s band were then investigated for associated electrons, using the lead converter of the detector. The result is shown in fig.26, where the visible cross section for $K^0_s e$ - production is plotted vs. $\sqrt{s}$ from 3.6 to 4.4 GeV. There is a strong signal around 4.05 GeV, 6 standart deviations above the background at 3.6 GeV, which repeats the step seen in the total cross section (chapter II). After corrections the cross section for associated $K^0 e$ - production was estimated at the peak as $\sigma(e^+e^- \to K^0 e^\pm + \text{anything}) \approx 3 \pm 1$ nb.

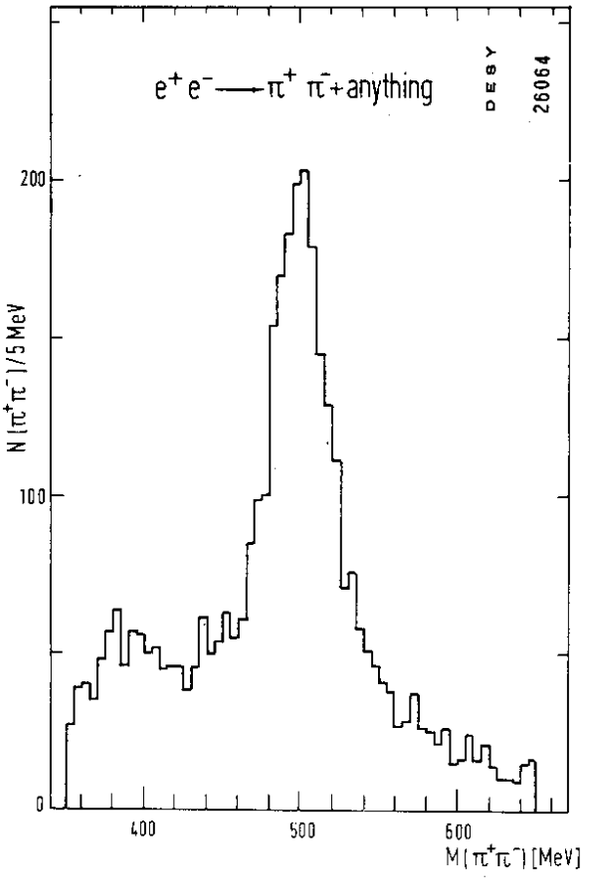

Fig.25 Invariant $\pi^+\pi^-$ mass for piors missing the interaction point.

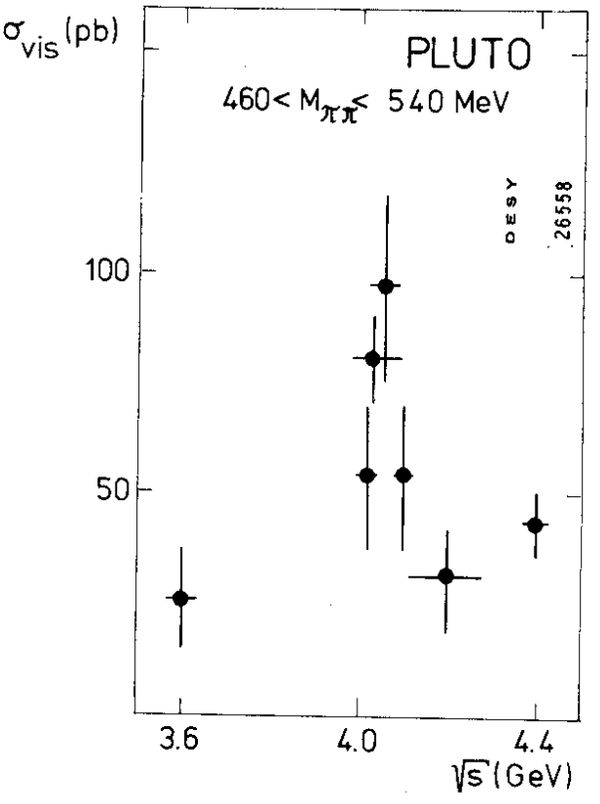

Fig.26 Visible cross section for $K^0_s e$ - events vs. $\sqrt{s}$.

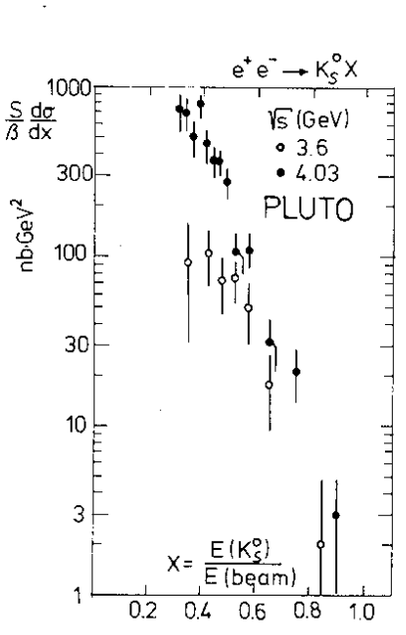

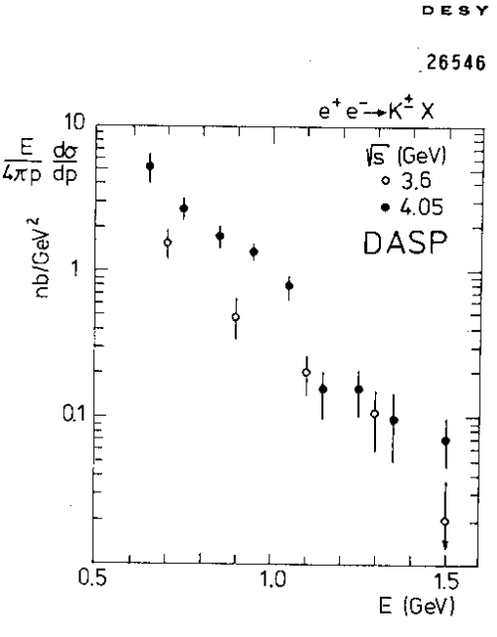

Fig.27
Inclusive kaon spectra. Left: K^0_s Right: $K^\pm$

Inclusive spectra for kaon production were measured in the PLUTO detector [26] for neutral kaons (K^o_s) and in the DASP detector [27] for charged kaons ($K^{\pm}$). The result is shown in fig.27, where the spectra taken at energies $\sqrt{s}$ = 3.6 are compared to those taken at $\sqrt{s}$ = 4.03 (4.05), the first resonance. Both experiments verify that the increase in kaon production beyond $\sqrt{s}$ = 4.0 GeV comes from the low energy kaons, $E_K \lesssim E_{beam}/2$. This behaviour confirms the expectation that, with two charmed mesons produced at threshold, each carries roughly the beam energy, and about half of this energy or less is left for the decay kaon. Data were analysed between $\sqrt{s}$ = 3.6 and 5.0 GeV, and fig.28a shows the inclusive cross section for kaon production in this energy range. In a simple model we expect production of K^+K^-, K^o_s, K^o_L in the ratio 1:1:1:1; the cross sections given in the figure are normalised to K^o_s. Both measurement agree well and show a strong increase of kaon prod= uction above 4.0 GeV, like the total cross section. The dashed line indicates the contribution from the "old" physics. With fig.28b an attempt is made to relate the excess of kaon production, R_K^{new}, to the excess in total cross section, R^{new} (not including the heavy lepton, see fig.14 for definition), in order to estimate the number of kaons per new event. The average of this ratio above $\sqrt{s}$ = 4.0 GeV is 0.39 ± 0.06 for K^o_s- production, the number of kaons per event is therefore four times larger: 1.56 ± 0.24, which comes close to the projected number of 2.

Another approach to reveal open charm is the investigation of the inclusive electron spectra. This has been done with the DASP spectrometer [28]. The original electron identification was improved for this purpose by adding Cerenkov counters (see fig.3). In fig.29 the observed number of charged prongs (including the electron) is plotted with and without photons for two energy intervals. After corrections, the analysis yields a very high average charged multiplicity, as indicated in the figure. Both energy intervals agree in this respect and also in the very high content of two prongs (cross hatched area). The authors seperate now the class of two prongs without photons, and investigate the rest for characteristic features of charm. One of these features is the copious production of kaons by virtue of the GIM current, which can be compared experimentally to kaon -

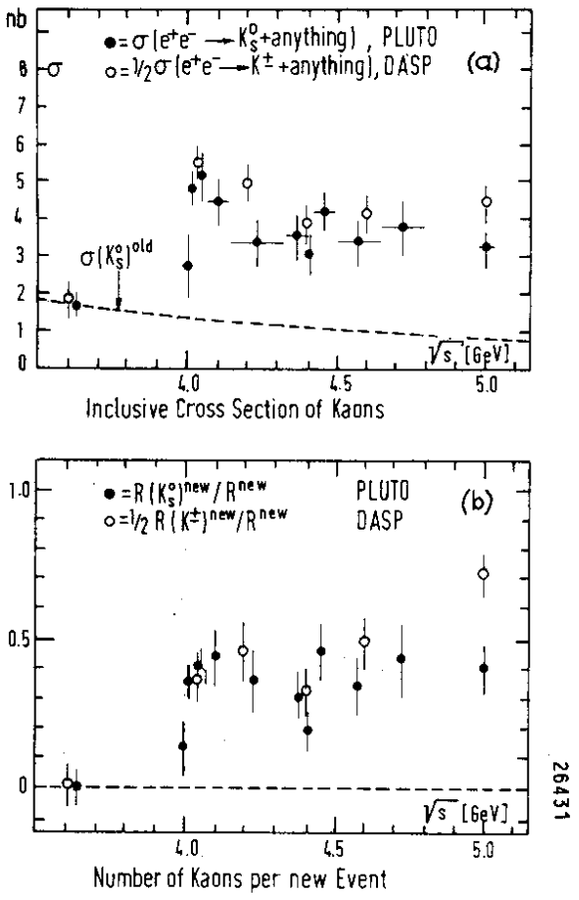

Fig.28 Inclusive kaon cross section (a) and its ratio to the new total cross section (b) versus $\sqrt{s}$.

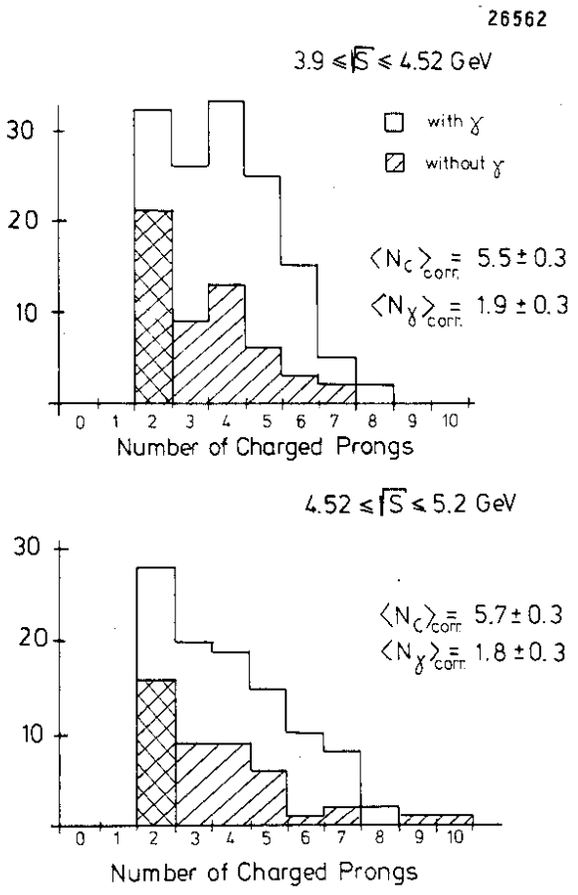

Fig.29 Experimental distribution of prong classes for two energy intervals, DASP detector.

production from the normal Cabbibo current. This was done by observing an identified charged hadron (π, K or $\bar{p}$) in the spectrometer arm, and an electron in the inner detector of the double arm spectrometer . The corrected ratio for the number of events eKX to the number of events eπX for the multiprong class was found to be $R_{K\pi} = 0.25 \pm 0.06$, but only 0.06 ± 0.06 for the two prong class. Using the measured charged multiplicity of $\langle n_{ch} \rangle = 5.5$ the conclusion is that each event of the multiprong class contains on the average 0.90 ± 0.18 charged kaons/event, equivalent to 0.45 ± 0.09 K^0_s/event, and in good agreement with the number derived from the inclusive kaon cross sections, fig.28. The two prong class, however, contains an average of only 0.07 ± 0.06 kaons/event consistent with the normal Cabbibo current. Fig.30 shows the inclusive electron spectrum for the multiprong class in the energy region of the first resonance at 4.03 GeV. The expected soft character of the spectrum is confirmed, $p_e < 1$ GeV/c. The solid curve represents the predicted spectrum [29] of electrons from the decay $D \rightarrow K^*(892)e\bar{\nu}$, which is favoured over other decays. The total cross section for inclusive electron production $e^+e^- \rightarrow e^\pm + X$, where X contains at least two charged tracks and any number of photons, is plotted in fig.31a as function of energy. Radiative corrections, a background subtraction, and a subtraction of the contribution from a heavy sequential lepton have been made. Note the large cross section at $\sqrt{s} = 4.03$ GeV of 2.1 nb, which corresponds to the peak in the cross section for K^0e - events measured earlier by the PLUTO collaboration, fig.26. The average semileptonic branching ratio for charmed hadrons is plotted as function of energy in fig.31b. It has been obtained by dividing the inclusive electron cross section by twice the cross section for charmed hadron production derived from the PLUTO data, marked as R^{new} in fig.14. The branching ratio of fig.31b is nearly independent of energy, and has an average BR($c \rightarrow e\bar{\nu}X$) = 0.11 ± 0.03. An independent determination of that number, which does not use the charm cross section, is obtained from a fraction of events, where a second electron was seen (27 events). These events lead to BR($c \rightarrow e\bar{\nu}X$) = 0.16 ± 0.06 in agreement with the value above.

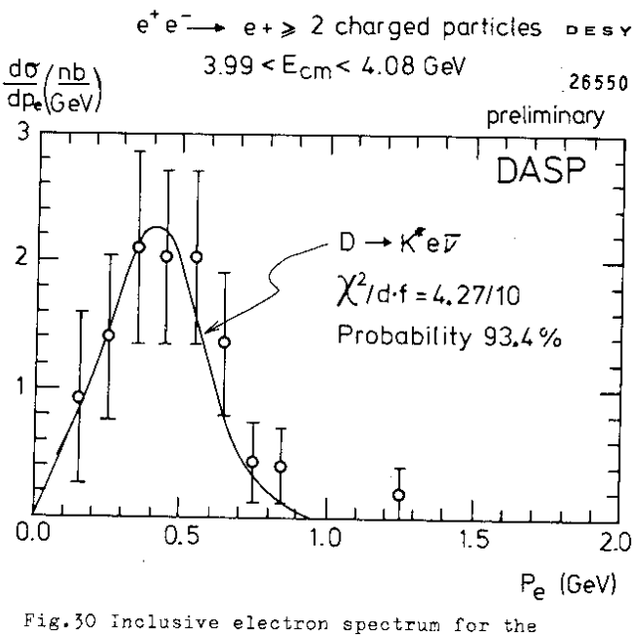

Fig.30 Inclusive electron spectrum for the multiprong class $n_{ch} \geq 2$ + photons.

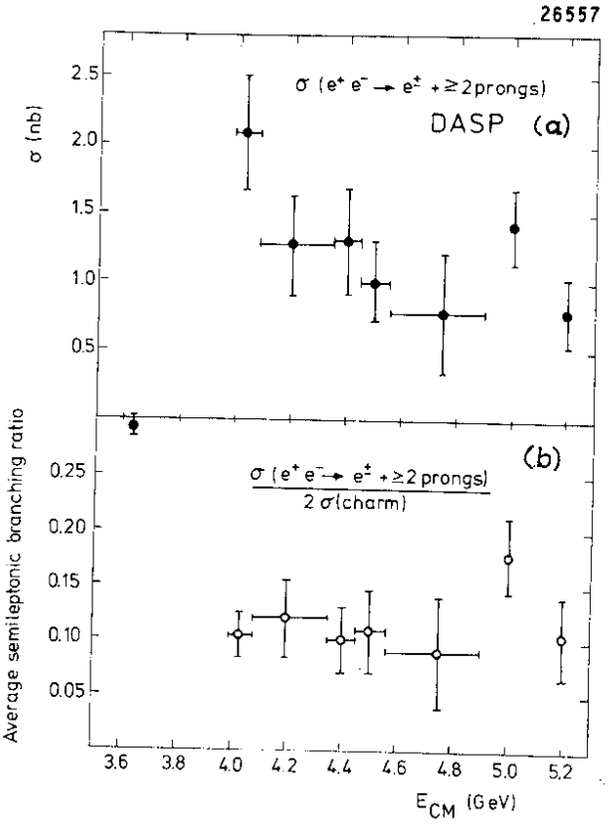

Fig.31 Inclusive electron cross section (a) and semileptonic branching ratio (b) versus $\sqrt{s}$

The first evidence for the F - meson was obtained recently in the DASP detector [30] by observing inclusive η- production between $\sqrt{s}$ = 4.0 and 5.2 GeV. While the D - mesons have been identified by invariant mass [16] and semileptonic decays [25)26)27)28] the F - mesons have so far escaped detection. The lowest mass member of the $c\bar{s}$ - mesons should have a weak decay predominantly into an $s\bar{s}$ - system, leading to final states with $K\bar{K}$, ϕ, η, or η'. The first excited state F* is predicted to be so close to the F, that $F^* \rightarrow \gamma F$ is the only possible decay channel, since both F and F* are isosinglets. The energy of the photon is expected to be $\sim$0.1 GeV [31]. The experiment was done mainly with the inner detector, shown in fig.3. The detection efficiency for photons was 50% at 0.05 GeV, 80% at 0.10 GeV and 95% above 0.30 GeV, without regard of the geometrical acceptance. The energy resolution of the shower counters was $\sigma(E) = 0.14/\sqrt{E}$ in GeV for $E > 0.05$ GeV. The resulting rms invariant mass resolution is 0.05 to 0.10 GeV in the region of the π^0, and is 0.08 in the region of the η. Events were required to have more than one charged track from the interaction point, and more than one photon with energies >0.10 GeV. Any two photons are used for the invariant mass $M_{\gamma\gamma}$, with their vector sum enclosed between 0.3 and 1.2 GeV/c. An additional photon of less than 0.14 GeV energy is called γ_{low}. Fig.32a shows the ratio measured of events with such an additional γ_{low} over those without versus the invariant mass $M_{\gamma\gamma}$ for five energies, centered around $\sqrt{s}$ = 4.0, 4.15, 4.4, 4.5, and 5.1 GeV. There is a peak at the η mass for $\sqrt{s}$ = 4.4 GeV, indicating that η production is correlated with a low energy photon. If the events without γ_{low} are considered as background, one arrives at 71 $\pm$ 17 events $\eta+\gamma_{low}$ observed at 4.4 GeV, corresponding to a visible cross section of 0.29 $\pm$ 0.07 nb. Fig.32b shows the distribution $M_{\gamma\gamma}$ for events with γ_{low}, again for the five energy intervals. The solid line represents a smoothed background. A π^0- peak is seen at all energies, but an η- peak only at 4.4 GeV. The shaded area is obtained by more stringent cuts to the photons. 60 $\pm$ 14 events $\eta+\gamma_{low}$ are counted above the background, corresponding to a visible cross section of 0.24 $\pm$ 0.06 nb. This cross section is plotted for all five energies in fig.33, comparing the two methods. An estimate of the detection efficiency for $\eta+\gamma_{low}$ indicates that the true cross section is a few nanobarns, corresponding to $\sim$one unit in R in the total cross section, which is a substancial fraction of the $\psi(4.4)$ cross section.

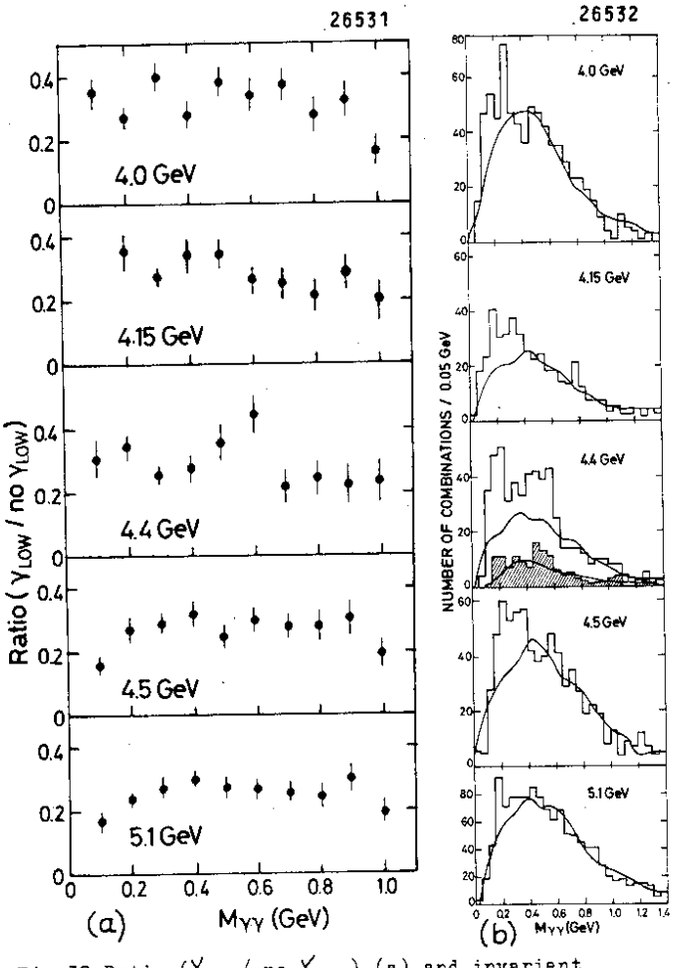

Fig.32 Ratio (γ_{low}/ no γ_{low}) (a), and invariant mass distribution $M_{\gamma\gamma}$ (b), for five energies.

The occurance of η production with low energy photons at 4.4 Gev strongly suggests the formation of $F\bar{F}^*$ or $F^*\bar{F}^*$. A search for the two body decay $F^{\pm} \rightarrow \eta\pi^{\pm}$ was performed by detecting the pion in one of the spectrometer arms, and asking for two photons to form the η mass and an additional low energy photon in the inner detector. 19 events of this type were found, three of these with two η's and three with two γ_{low}'s. The events were fitted either to the reaction

(1) $e^+e^- \rightarrow F\gamma_{low}F^{\pm} \rightarrow F\gamma_{low}\pi^{\pm}\eta$ or to

(2) $e^+e^- \rightarrow F^*F^{\pm *} \rightarrow F^*\gamma_{low}F^{\pm} \rightarrow F^*\gamma_{low}\pi^{\pm}\eta$.

Six events gave a fit to hypothesis (1) with $\chi^2 < 10$. These are shown in fig.34 as scatter plot of the fitted mass $M(\pi\eta)$ versus the recoil mass. Four events cluster around $m_{\pi\eta}$ = 2.04 GeV and m_{recoil} = 2.17 GeV. Only these six events gave also an acceptable fit to hypothesis (2) with $m_{\pi\eta}$ = 2.01 and m_{F^*} = 2.11 GeV. The best estimates for the masses are m_F = 2.03$\pm$0.06 and m_{F^*} = 2.14$\pm$0.06 GeV.

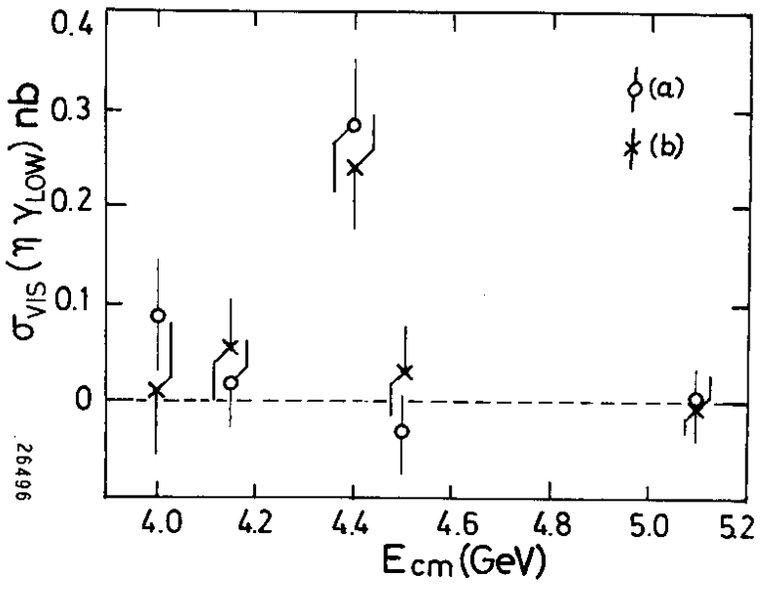

Fig.33 Visible cross section for production of $\eta+\gamma_{low}$ as function of $\sqrt{s}$. See fig.32 for the two methods (a) and (b)

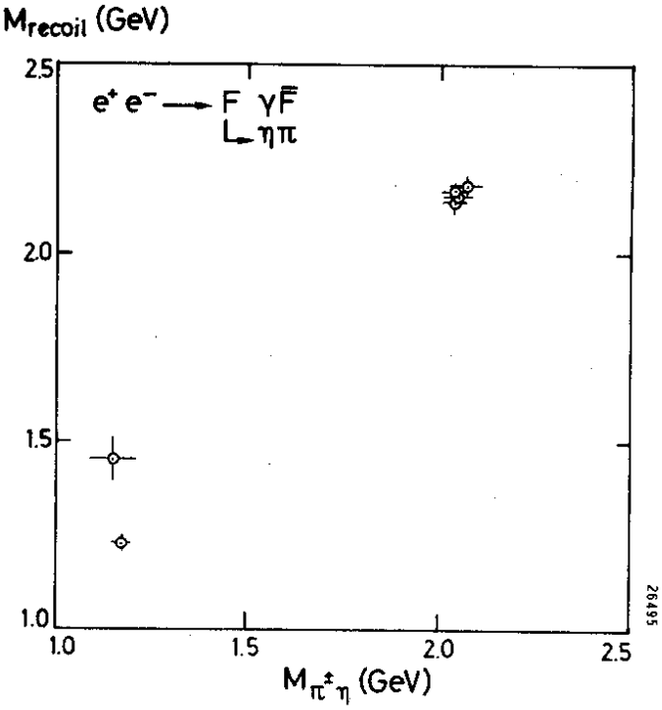

Fig.34 Fitted mass vs. recoil mass

V. Experimental Evidence for the heavy Lepton τ at DORIS

Since the first results on e/μ final states in e^+e^- annihilation, obtained at SPEAR [32] there has been increasing evidence for the existance of a new heavy lepton from DORIS- and SPEAR-experiments [33]. The evidence from DORIS experiments stems from four different final state channels: inclusive muon spectra and electron-muon events were observed in the PLUTO detector, inclusive electron spectra and the eK/eπ - ratio for twoprong events were measured in the DASP spectrometer.

Table 4
Decays of τ^- for $m_\tau = 1.9$ GeV/c^2

decay mode	branching ratio	number of prongs
$\nu_\tau e^- \bar{\nu}_e$	.20	1
$\nu_\tau \mu^- \bar{\nu}_\mu$	.20	1
$\nu_\tau \pi^-$	.11	1
$\nu_\tau K^-$	.01	1
$\nu_\tau \rho^-$	.22	1
$\nu_\tau K^{*-}$	.01	1
$\nu_\tau A_1^-$	.07	1,3
ν_τ n·h	.18	1,3,5

The experimental evidence reported here will be compared with the model of a sequential heavy lepton [34], called τ. This lepton continues the sequence of the known leptons : ν_e,e / ν_μ,μ / ν_τ, τ and thus has its own massless left-handed neutrino, has spin 1/2, and is produced in e^+e^- annihilation in pairs like a pointlike fermion with the cross section $\sigma_{\tau\tau} = \sigma_{\mu\mu}(3\beta - \beta^3)/2$, where β is the velocity of τ (for $\sigma_{\mu\mu}$ see fig.14). For $\beta \rightarrow 1$ it adds one unit of R to the total annihilation cross section, as indicated in fig.14. The decay scheme of τ has been calculated by many authors [35], assuming a conventional V-A coupling of τ and ν_τ to the usual weak current. A list of decay modes and branching ratios based on a mass $m_\tau = 1.9$ GeV/c^2 is given in table 4. It is remarkable that the dominant fraction of final states contain only one charged particle, BR(1)≈85%, we therefore expect a high fraction of two prongs from a decaying pair: BR(1)·BR(1)≈ 70%. Also, a high percentage of the decays are purely leptonic, BR(e)+BR( )≈40%. The chance to see two leptonic decays (i.e. e/μ, /μe, ee, and /μ/μ) in an event is≈16%.

We start with discussing the inclusive muon- and e/μ-experiments with the PLUTO detector [36]. The high percentage of twoprongs in the total cross section observed in PLUTO [14] do in fact find its most natural explanation in the assumption of a new object which favours to feed this prong class, compare fig.17. To find more evidence for this conjecture, that fraction of twoprongs containing a muon was separated. Because of its compact iron yoke and the resulting short decay path for pions or kaons, the superconductive detector PLUTO is particularely suited to identify muons behind the iron yoke which absorbs the hadrons. The measured percentage of hadrons misidentified as muons is reported $P_{h\to\mu} = 2.8\pm0.7$ % (punchthrough and decay). The hadron absorber causes a momentum cutoff at $p_\mu > 1.0$ GeV/c, and the solid angle used for muon detection was $\Delta\Omega_\mu = 0.43\cdot4\pi$, by the restriction $|\cos\theta|<0.75$. The second track was limited to $p>0.24$ GeV/c and $|\cos\theta|<0.87$. Any number of photons were admitted. The twoprong class thus defined, $e^+e^-\to \mu^\pm$ + 1pr + n·γ, has background from four sources : $e^+e^-\to\mu\mu$, $\mu\mu\gamma$, $\mu\mu\gamma\gamma$; $h\to\mu$. The first is large but easy to remove by an acoplanarity cut, the last two sources are rather small and known from measurement: $P_{h\to\mu}$, or calculation: $\mu\mu\gamma\gamma$ [37]. The second contribution is again large, and is removed by a cut in the squared missing mass as shown in fig.35. The applied cut is energy dependent and can be controlled by the fact that a large part of the $\mu\mu\gamma$ events are seen in the detector (shaded area). After subtraction of the backgrounds the resulting muon spectra above the cutoff momentum are shown in fig.36 for three energy intervals. The figure contains 215 events obtained with an integrated luminosity of 5700 nb^{-1}. The spectra display two features which are characteristic for the decay. Firstly, they move with increasing center of mass energy to higher momenta,which is typical for the decay from a pair of fixed mass particles (Lorentz boost).

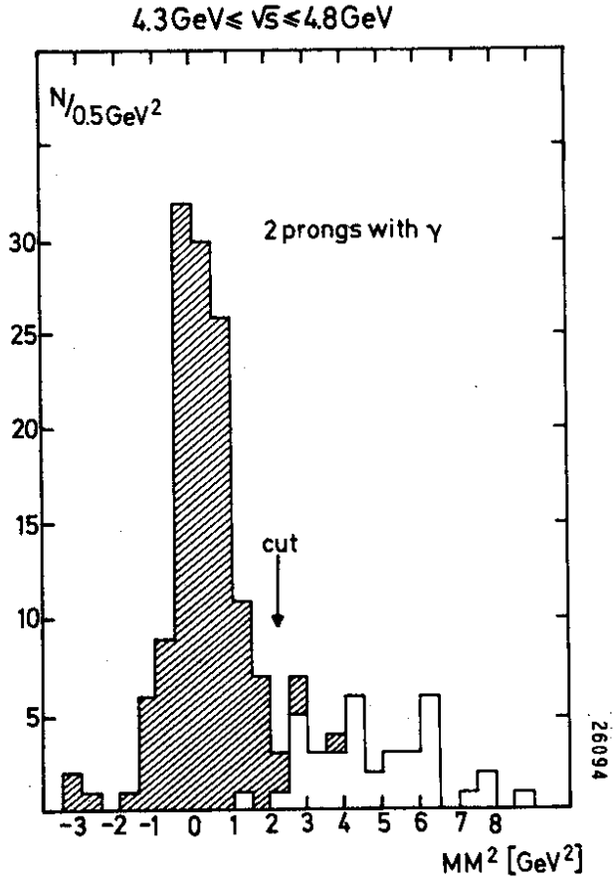

Fig.35 Square of missing mass for twoprong events with one converted photon.Shaded area: the photon conversion point is consistent with missing momentum direction.

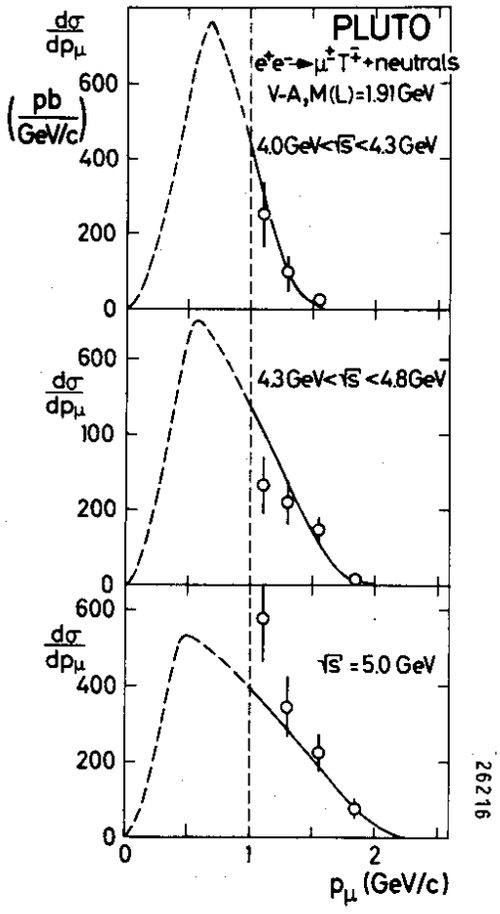

Fig.36 Muon momentum distribution, cross section corrected for trigger and acceptance.

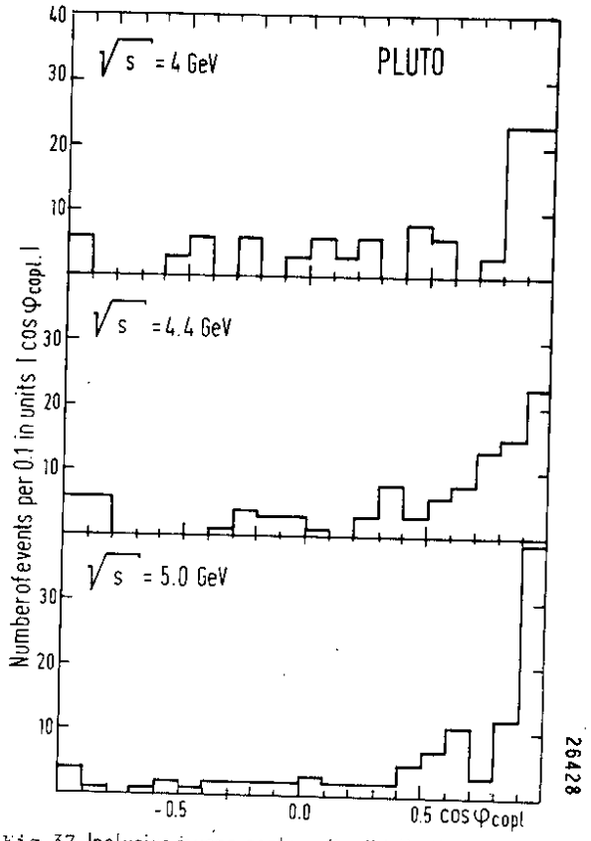

Fig.37 Inclusive muons, coplanarity distribution Two prongs

Table 5

Fits to inclusive muon spectra

spin	decay	$m(\nu_\tau)$	m_τ	BR(1) BR(μ)	χ^2/DF
0	$\sim K_{\ell 3}$	0	1.67 ± 0.08	1.35 ± 0.29	6.5/9
1/2	V-A	0.5	1.72 ± 0.09	$.130\pm0.017$	22.5/9
1/2	V+A	0	1.79 ± 0.07	$.136\pm0.019$	15.1/9
1/2	V-A	0	1.91 ± 0.03	$.109\pm0.012$	10.3/9

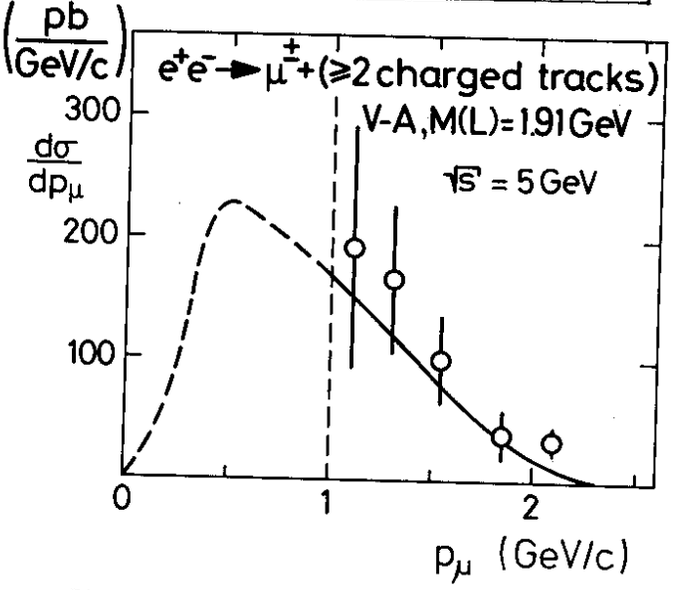

Fig.38 Inclusive muon spectrum for multiprongs

This can also be shown by the coplanarity distribution of the twoprongs as plotted in fig.37 for the three energies, because it shrinks when the decay particles are forced back to back by increasing energy. Secondly, the finite slope of the spectrum, which requires a triangular shape in the unobserved region $p_\mu < 1$ GeV/c, is incompatible with a twobody decay, but agrees with the threebody decay $\tau \to \nu_\tau \bar{\nu}_\mu \mu$ of the heavy lepton. There is a large missing mass of typically 2.5 GeV/c^2 in the events, as can be seen from fig.37. Of the 215 twoprong events, 85 have a photon and 130 have no observed photon. The average number of photons observed per twoprong event is $\langle n_\gamma \rangle < 0.7$, which rules out, that a π^0 or η are among the missing neutral particles, because for their two photon decays $\langle n_\gamma \rangle \approx 1.2$ is expected.

The spectra of fig.36 have been fitted to the τ model by varying spin, coupling, and neutrino mass. The result is presented in table 5. The spin zero assignment can be ruled out (Higgs boson?), even though the χ^2 is smallest, because the resulting branching product leads to an unphysical branching ratio BR(μ) $\approx$ 100%. The large χ^2 of the next fit with $m(\nu_\tau) = 0.5$ GeV/c^2 excludes the assumption that a new baryon is observed, which decays into $n + \mu + \nu$. Among the last two fits the V-A coupling is favoured. This fit is represented by the solid lines in fig.36. The resulting mass is then $m_\tau = 1.91 \pm 0.03$ GeV/c^2.

In order to determine the branching ratio into muons the multiprong class $\mu + \geq 2$pr was measured and compared to the class μ+1pr+nγ at $\sqrt{s} = 5$ GeV. The spectrum is presented in fig.38 for this energy, but the line shown is a fit to the data at all CMS-energies (108 events) with the parameters of table 5, line 4. The comparison yields BR(1) = 0.70 ± 0.10, BR(≥ 2) = 0.30 ± 0.10, which can be used to extract BR(μ) by dividing the product of branching ratios of table 5 by BR(1), with the result BR(μ) = 0.15 ± 0.03.

We turn now to the twoprong class in the inclusive electron spectra observed in the DASP inner detector (fig.29) and look at the spectrum of these electrons [38], shown in fig.39. It reaches up to 2 GeV/c in striking contrast to the electron spectrum of the respective multiprong class (fig.30). The

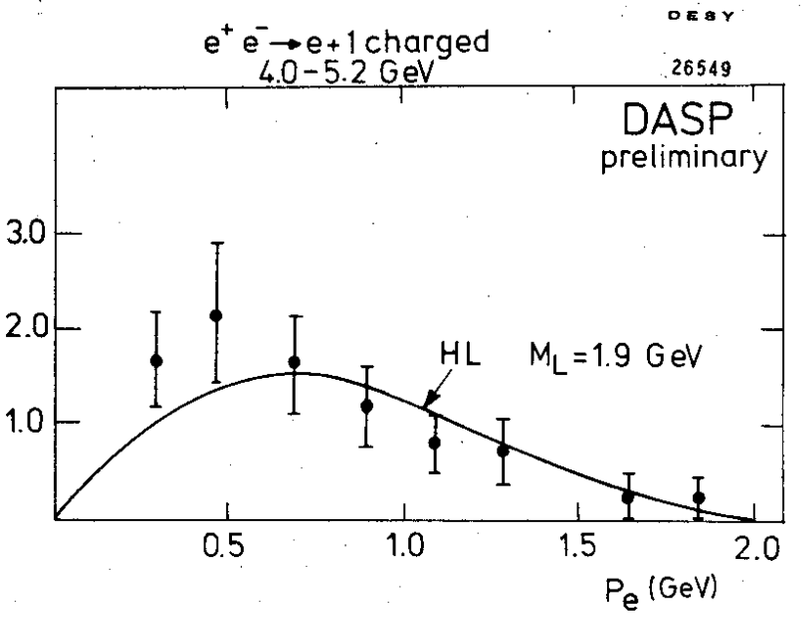

Fig.39 Inclusive electron spectrum for the twoprongs, DASP

solid line indicates further that the spectrum is compatible with the heavy lepton hypothethis. Going back to chapter IV we find more support for the conclusion, that the events of the twoprong class are dominantly from another source than charm, in the measured ratio of 0.07 ± 0.06 kaons/event, which is again in agreement with what is expected from the decay $\tau^- \rightarrow \nu_\tau K^-$, table 4. Also the energy dependence of cross section for inclusive electrons, found by integration of the spectra, is in gross agreement with the heavy lepton hypothesis as indicated in fig.40.

The most selective signature for detecting the τ is the e/μ - channel, which at the same time yields the smallest cross sections. 23 of these events have been observed in the PLUTO detector [39] with the integrated luminosity already mentioned. Fig.41 shows one event e^+/μ^- where the electron radiates in the first lead converter and the photon showers in the second converter. The efficiency to detect electrons rises from 20% at 0.3 GeV/c to 80% above 0.7 GeV/c. The probability to misidentify a hadron as electron was measured $P_{h \rightarrow e} = 3.5 \pm 0.7$ %. The photon detection efficiency was 80%. The result of a search for e/μ - events is shown in table 6. Six events $\mu^+\mu^-$ have been found, which are in agreement with the expectation (high momentum cut). No e/μ - events with like sign have been seen. The observed numbers of e/μ - events with photons or charged tracks are compatible with background estimates. In particular it is estimated that the contribution of charm events to the 23 e/μ - events could be at most two events. The branching ratio for electrons is obtained by comparing the cross section for e/μ + nothing with the inclusive muon cross sections, shown in fig.42.

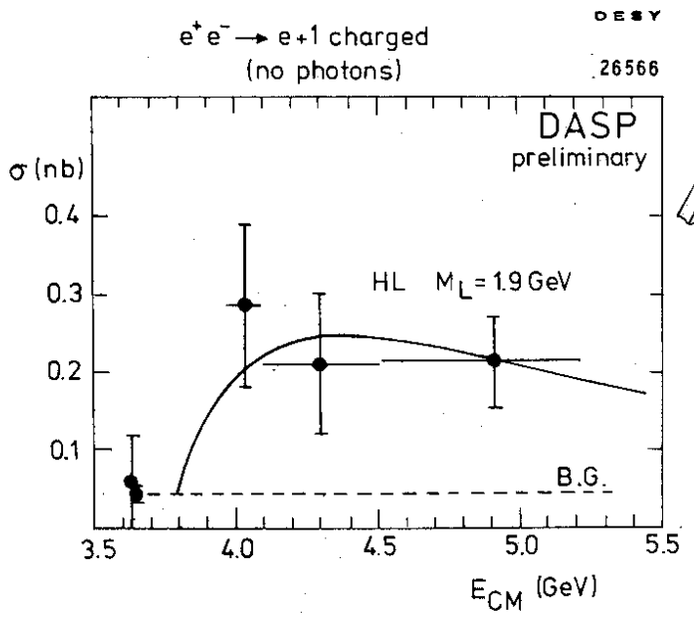

Fig.40 Cross section for inclusive electrons versus $\sqrt{s}$ for the twoprong class, DASP

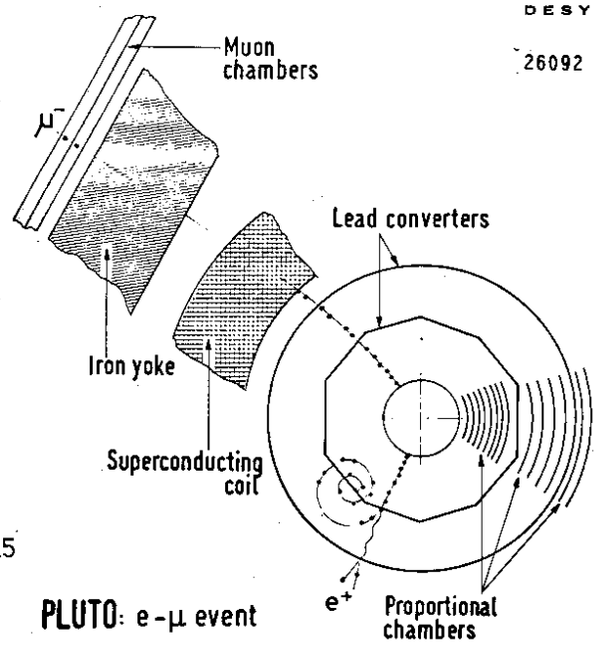

Fig.41 Electron-muon event in PLUTO

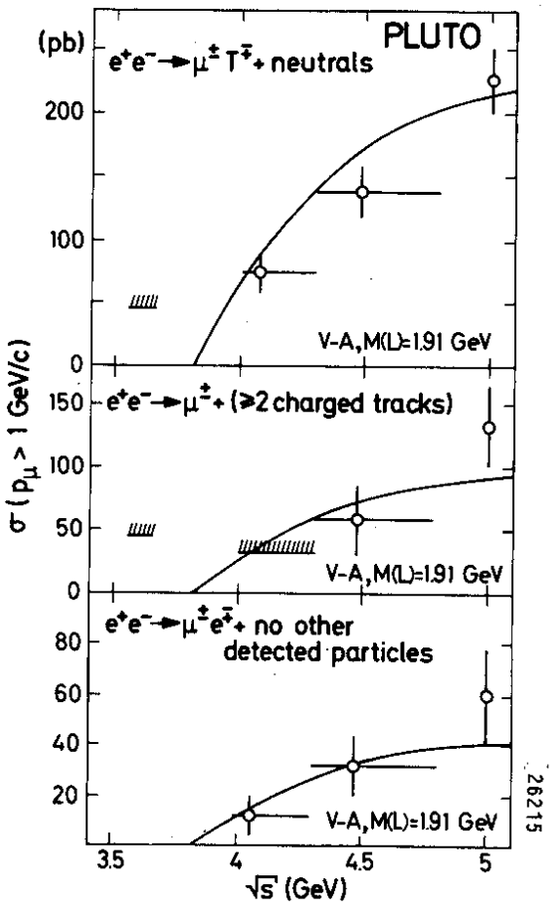

Fig.42 Comparison for cross sections for $e^+e^- \to e/u$, $/u + \geq 2pr$, $/u + 1pr + n\cdot\gamma$ vs. $\sqrt{s}$; corrections are applied except for the momenta $p_{/\mu} < 1$ GeV/c.

Table 6

e/u - and $/u/u$ - events and backgrounds, for $4.0 < \sqrt{s} < 5.0$ GeV.

event signature	number of events	back= ground	visible cross section
$e^{\pm}/u^{\mp}$	23	2	33 pb
$/u^+/u^-$	6	0	8 pb
$e^{\pm}/u^{\pm}$	0	0	0 pb
$e^{\pm}/u^{\mp} + n\cdot\gamma$	4	2	5 pb
$e^{\pm}/u^{\mp} + \geq 1pr$	7	8	0

Note that all three cross sections have the same threshold behaviour, so that we conclude they also have the same origin. The solid curves are again calculated with the parameters of table 5, line 4. The comparison yields a branching ratio $BR(e) = 0.14 \pm 0.04$. A final evidence in support of the heavy lepton hypothesis is given by the experimental spectrum of these electrons, presented in fig.43. The comparing curve takes the decaying detection efficiency for electrons at low momenta into account. It confirms again the compatability with the τ- conjecture.

Summing up the experimental evidence for the new heavy lepton τ from PLUTO - and DASP - experiments we find the following features in agreement with the properties of the model outlined in table 4:

(1) The object is produced in pairs, as seen by the boost of the inclusive muon spectra with energy;

(2) It has the expected threshold behaviour, seen in four final state channels: $/u$-inclusive for

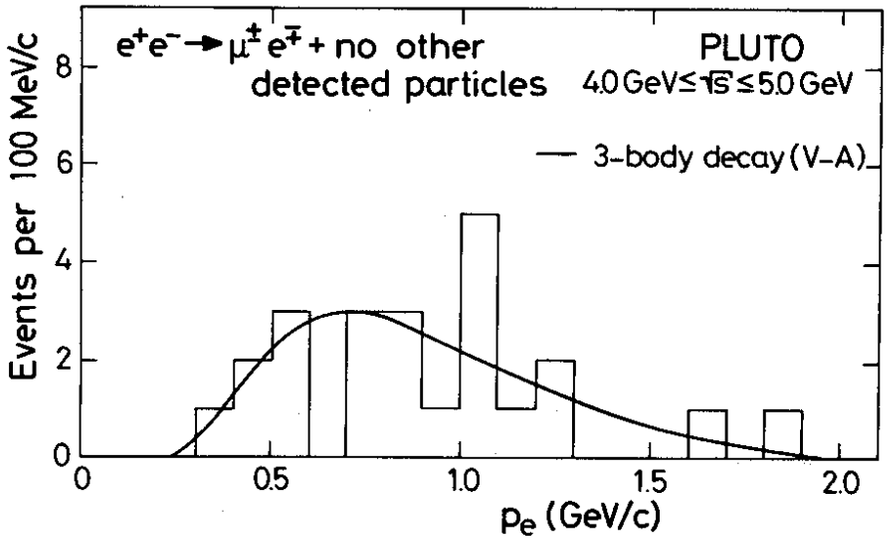

Fig.43 Experimental electron spectrum of the e/u - events, compared with the expectation

twoprongs, μ-inclusive for multiprongs, e-inclusive for twoprongs, and e/μ, which implies that a pointlike particle is produced,
(3) Spin 1/2 is very likely because spin zero is ruled out,
(4) The muon- and electron-spectra show the expected threebody decay,
(5) The measured branching ratios for muons, electrons, and kaons are in agreement with the model,
(6) The weak coupling V-A is favoured,
(7) The neutrino mass is < 0.5 GeV/c^2, but π^0 or η are ruled out as missing neutral particle.

We conclude that the observed object is in fact identical with the sequential heavy lepton τ. For the exclusion of other hypothetic objects with similar signatures, like paraleptons, ortholeptons etc., by the present experimental evidence see ref. [40]. The complete evidence for the new sequential lepton, however, still lacks a proof that V+A is excluded, its needs a measurement of its lifetime, and requires more information about the neutrino mass and its lepton number.

Acknowledgement: I thank my collegues of the experimental groups at DORIS, who have helped to prepare this review in any possible way, and apologize for not quoting names in lack of a suitable selection criterium.

References

1) DASP-Collaboration, W.Braunschweig et al., Phys.Lett.67B,243(1977)
2) W.Bartel et al., Phys.Lett.64B,483(1976)
W.Bartel et al., Phys.Lett.66B,489(1977)
3) S.Okubo, Phys.Lett.5,105(1963)
G.Zweig, CERN Report TH 401,412(1969)
J.Iizuka, K.Okada, O.Shito, Proc.Theor.Phys.35,1061(1966)
4) H.Harari, Phys.Lett.60B,172(1976)
A.Kazi, G.Kramer, D.H.Schiller, Acta Phys.Austr.45,65(1976)
A.Kazi, G.Kramer, D.H.Schiller, Acta Phys.Austr.45,195(1976)
A.Kazi, G.Kramer, D.H.Schiller, Lett.Nuovo Cimento15,120(1976)
5) T.Walsh, Nuovo Cimento Lett.14(1975)
R.N.Cahn, M.S.Chanowitz, Phys.Lett.59B,277(1975)
6) E.Pelaquier, F.M.Renard, Nuovo Cimento 32A,421(1976)
7) DASP-Collaboration, W.Braunschweig et al., Phys.Lett.67B,249(1977)
8) DASP-Collaboration, W.Braunschweig et al., Phys.Lett.57B,407(1975)
9) J.S.Whitaker et al., Phys.Rev.Lett.37,1596(1976)
10) C.J.Biddick et al., Phys.Rev.Lett.38,1324(1977)
11) PLUTO-Collaboration: V.Blobel, Proc.of the XIIth Rencontre de Moriond, Flaine ,March 1977
12) PLUTO-Collaboration, J.Burmester et al., Phys.Lett.68B,283(1977)
13) C.Rosenzweig, Phys.Rev.Lett.36,697(1976)
M.Bander et al., Phys.Rev.Lett.36,695(1976)
A.de Rújula et al., Phys.Rev.Lett.38,317(1977)
14) PLUTO-Collaboration, J.Burmester et al., Phys.Lett.66B,395(1977)
15) G.Hanson et al., Phys.Rev.Lett.35,1609(1975)
P.Grassberger, E.H.de Groot, Nucl.Phys.B102,297(1976)
16) G.Goldhaber et al., Phys.Rev.Lett.37,255(1976)
I.Peruzzi et al., Phys.Rev.Lett.37,569(1976)
J.E.Wiss et al.,Phys.Rev.Lett.37,1531(1976)
17) J.Siegrist et al., Phys.Rev.Lett.36,700(1976)
18) DASP-Collaboration, R.Brandelik etal., Phys.Lett.67B,358(1977)
19) G.G.Hanson, Talk given at the XVIIIth Int.Conf.on High Energy Physics, Tiblisi, USSR(1976); SLAC-PUB-1814(1976)
20) PLUTO-Collaboration, to be published

References(continued)

21) G.Jansco et al., Nucl.Phys.B124,1(1977) and A.Zieminski,Invited Talk at the EPS European Conf. on Particle Physics, Budapest(1977)
22) V.V.Anisowich, V.M.Shekhter, Nucl.Phys.B55,455(1973)
23) Y.Hara, Phys.Rev.B134,701(1964)
J.D.Bjorken, S.L.Glashow, Phys.Lett.11,255(1964)
24) S.L.Glashow, J.Iliopoulos, L.Maiani, Phys.Rev.D2,1285(1970)
25) PLUTO-Collaboration, J.Burmester et al.,Phys.Lett.64B,369(1976)
26) PLUTO-Collaboration, J.Burmester et al.,Phys.Lett.67B,367(1977)
27) DASP-Collaboration, R.Brandelik et al., Phys.Lett.67B,363(1977)
28) DASP-Collaboration, W.Braunschweig et al., Phys.Lett.63B,471(1976)
DASP-Collaboration, R.Brandelik et al., DESY 77/36, to be published in Phys.Lett.
DASP-Collaboration, R.Brandelik et al., DESY 77/41, to be published in Phys.Lett.
29) A.Ali, T.C.Yang, Phys.Lett.65B,275(1977)
30) DASP-Collaboration, R.Brandelik et al., DESY 77/44, submitted to Phys.Lett.
31) c.f. M.K.Gaillard, B.W.Lee, J.L.Rosner, Rev.Mod.Phys.47,277(1975)
32) M.L.Perl et al., Phys.Rev.Lett.35,1489(1975)
33) M.L.Perl et al., Phys.Rev.Lett.38,117(1976)
G.J.Feldmann et al., Phys.Lett.63B,466(1976)
M.Cavalli-Sforza et al., Phys.Rev.Lett.36,588(1976)
D.H.Badtke et al., Paper presented at the Washington Meeting of the APS(April 1977)
A.Barbaro-Galtieri et al., LBL-6458(June 1977), and
A.H.Litke, Invited Talk at the EPS European Conf. on Particle Physics, Budapest 1977
34) M.L.Perl, P.Rapidis, SLAC-PUB-1496(1974), with early references
35) Y.S.Tsai, Phys.Rev.D4,2821(1971)
H.B.Thacker,J.J.Sakurai, Phys.Lett.36B,103(1971)
J.D.Bjorken, C.H.Llewellyn Smith, Phys.Rev.D7,887(1973)
K.Fujikawa, N.Kawamoto, Phys.Rev.D14,59(1976)
36) PLUTO-Collaboration:H.Meyer, Proceedings of the Orbis Scientiae, Coral Gables(Jan.1977) and DESY 77/19
PLUTO-Collaboration, J.Burmester etal., Phys.Lett.68B,297(1977)
37) F.Cutbrodt, Z.J.Rek, DESY 77/45
38) DASP-Collaboration: R.Kotthaus, Paper presented at the Aachen Meeting of the DPG(March 1977)
39) PLUTO-Collaboration, J.Burmester et al., Phys.Lett.68B,301(1977)
40) PLUTO-Collaboration: C.Flügge, Proceedings of the Vth International Conf. on Experimental Meson Spectroskopy, North Eastern University, Boston(April 1977) and DESY 77/35